nature medicine

ARTICLES

https://doi.org/10.1038/s41591-018-0299-9

Corrected: Publisher Correction

Cannabinoid CB_1 receptors in the amygdalar cholecystokinin glutamatergic afferents to nucleus accumbens modulate depressive-like behavior

Chen-Jie Shen, Di Zheng, Ke-Xin Li, Jian-Ming Yang, Hao-Qi Pan, Xiao-Dan Yu, Jia-Yu Fu, Yi Zhu, Qi-Xin Sun, Meng-Yu Tang, Ying Zhang, Peng Sun, Yi Xie, Shumin Duan, Hailan Hu and Xiao-Ming Li*

Major depressive disorder is a devastating psychiatric disease that afflicts up to 17% of the world's population. Postmortem brain analyses and imaging studies of patients with depression have implicated basal lateral amygdala (BLA) dysfunction in the pathophysiology of depression. However, the circuit and molecular mechanisms through which BLA neurons modulate depressive behavior are largely uncharacterized. Here, in mice, we identified that BLA cholecystokinin (CCK) glutamatergic neurons mediated negative reinforcement via D2 medium spiny neurons (MSNs) in the nucleus accumbens (NAc) and that chronic social defeat selectively potentiated excitatory transmission of the CCK^{BLA}–$D2^{NAc}$ circuit in susceptible mice via reduction of presynaptic cannabinoid type-1 receptor (CB_1R). Knockdown of CB_1R in the CCK^{BLA}–$D2^{NAc}$ circuit elevated synaptic activity and promoted stress susceptibility. Notably, selective inhibition of the CCK^{BLA}–$D2^{NAc}$ circuit or administration of synthetic cannabinoids in the NAc was sufficient to produce antidepressant-like effects. Overall, our studies reveal the circuit and molecular mechanisms of depression.

The lifetime prevalence (~17%) and economic burden ($100 billion annually) associated with major depressive disorder (MDD) make it one of the most common and debilitating neurobiological illnesses worldwide[1–3]. Stress-induced neural plasticity changes in the brain's reward and aversion systems are strongly implicated in MDD[4–6]. Among several valence-coding brain regions, the BLA is prominent. Despite evidence from human studies implicating changes in volume[7], metabolism[8,9] and valence response[10] of the BLA in depressed patients, how BLA-related neural circuits are involved in the pathogenesis of depression remains largely unexplored.

A major downstream target of the BLA is the NAc[11,12]. Previous results are mixed regarding the valence of the BLA–NAc neural circuit[11–13], implying that there are at least two neural sub-circuits encoding opposite emotional valences. To understand the potential role of the BLA–NAc circuit in depression, it is critical to identify these specific sub-circuits and study how they are differentially regulated by stress.

Cannabinoid type-1 receptors (CB_1R) have been implicated in the regulation of mood and depression. Genetic deficiency[14–19] in, or antagonism[20] of, CB_1R can cause an increase in depressive-like behavior. One well-known case is that the anti-obesity drug rimonabant, a CB_1R antagonist, increases the risk of severe depression, which leads to market withdrawal in 2008[21]. In contrast, synthetic cannabinoids with agonist activity of the central CB_1R alleviated depressive-like symptoms in animal models[22,23]. However, the neural circuit mechanism mediating maladaptive CB_1R function in depression and the antidepressant effects of cannabinoids are unclear.

Here, we show that BLA cholecystokinin (CCK)-expressing excitatory input to the NAc core (NAcc) D2 medium spiny neurons (MSNs) transmitted negative valence and that social defeat stress selectively potentiated excitatory transmission of the CCK^{BLA}–$D2^{NAcc}$ circuit via downregulation of presynaptic CB_1R in susceptible mice. Moreover, cell type-specific knockdown of CB_1R in the CCK^{BLA}–$D2^{NAcc}$ circuit increased stress susceptibility and pharmacological activation of CB_1R in NAcc rescued depressive-like behavior in susceptible mice. These results suggest, for the first time, that downregulation of CB_1R in a CCK^{BLA}–$D2^{NAcc}$ circuit represents an endophenotype for stress-induced depression and points to an essential role of CB_1R within this circuit in promoting stress resilience.

Results

Using neuropeptide CCK as a genetic marker to subdivide BLA glutamatergic neurons mediating opposite emotional valance. The neuropeptide CCK is abundantly expressed in the amygdala[24–26]. To visualize CCK-expressing neurons, we crossed a mouse line expressing Cre recombinase under the control of the cholecystokinin promoter (CCK-ires-Cre) with a Cre-dependent tdTomato (tdT) reporter line (Ai14-LSL-tdT, Fig. 1a). We found a substantial population of CCK-positive neurons in the BLA of CCK-ires-Cre::Ai14 mice, and we also found that CCK-tdTomato cellular expression closely matched endogenous *Cck* messenger RNA (mRNA) expression (Fig. 1a and Extended Data Fig. 1a).

CCK neurons have long been considered as GABAergic and are known to mediate target-specific inhibition of pyramidal neurons[27,28]. To examine whether CCK-positive neurons in the BLA are also inhibitory GABAergic neurons, we performed immunofluorescence (Fig. 1c and Extended Data Fig. 1b) in CCK-ires-Cre::Ai14 mice. Surprisingly, unlike hippocampal GABAergic counterparts, we found that most (94.7%) CCK-positive neurons co-expressed the

Center for Neuroscience and Department of Neurology of Second Affiliated Hospital, NHC and CAMS Key Laboratory of Medical Neurobiology, Joint Institute for Genetics and Genome Medicine between Zhejiang University and University of Toronto, Zhejiang University School of Medicine, Hangzhou, China. *e-mail: lixm@zju.edu.cn

forebrain glutamatergic marker CaMKIIα, with only a small fraction (2.3%) expressing inhibitory GABAergic marker GAD67 (Fig. 1c,d). Furthermore, CCK neurons expressed neither the GABAergic marker parvalbumin nor somatostatin (Fig. 1c,d), suggesting that most CCK-positive neurons in the BLA are glutamatergic rather than GABAergic. In addition, we found that BLA CCK neuropeptidergic neurons account for 63.3% of BLA glutamatergic neurons, with the remaining 36.7% not co-localized with CCK-tdTomato (non-CCK) (Fig. 1e). These results drove our proposal that CCK and non-CCK glutamatergic neurons may represent distinct subpopulations in the BLA.

To investigate circuit-level differences between BLA CCK and non-CCK glutamatergic neurons, we initially applied an intersectional strategy by injecting an adeno-associated virus expressing CaMKIIα promoter-driven Cre-dependent ChR2-mCherry (CaMKIIα-Cre-on-ChR2-mCherry, Fig. 1f) into the BLA of CCK-ires-Cre mice (Cre-on mice). In parallel, to label BLA non-CCK glutamatergic neurons, we combined a CaMKIIα promoter with a 'Cre-out' strategy (Fig. 1i) in which Cre recombinase excises the ChR2-eYFP coding sequence[29]. We found a strong presence of both mCherry and eYFP signals in the NAcc (Fig. 1f,i and Extended Data Fig. 1c,d). However, BLA CCK neurons sent more abundant innervations to the NAc lateral shell, olfactory tubercle (Extended Data Fig. 1c,d) and ventral hippocampus (Extended Data Fig. 1e). On the basis of both BLA CCK and non-CCK glutamatergic neurons sending strong innervations to the NAcc, we selected this to further investigate the functionality of these two parallel BLA–NAc circuitries.

Next, we selectively activated $CCK^{BLA\text{-}NAcc}$ and non-$CCK^{BLA\text{-}NAcc}$ glutamatergic neurons by applying the above-mentioned intersectional Cre-on or Cre-out optogenetic strategies in real-time place preference (RTPP) or avoidance (RTPA) assays. Strikingly, optogenetic activation of the $CCK^{BLA\text{-}NAcc}$ circuit reduced the time spent in the chamber paired with light stimulation (Fig. 1g,h), indicating that activation of this circuit is aversive. To confirm this aversive effect, we optically activated the $CCK^{BLA\text{-}NAcc}$ circuit during sucrose reinforcement and found a decrease in the number of active nose pokes paired with sucrose (Fig. 1l,m). Optically evoked behavioral aversion in the RTPA was blocked by intra-NAcc local infusion of the α-amino-3-hydroxy-5-methyl-4-isoxazole propionate receptor (AMPAR) antagonist DNQX (1 μg in 200 nl each side), but not of CCK_A or CCK_B receptor antagonists L-364,718 or L-365,260 (0.1 or 1 μg in 200 nl each side) (Fig. 1h and Extended Data Fig. 1f). In contrast, optogenetic activation of the non-$CCK^{BLA\text{-}NAcc}$ circuit produced strong reinforced behavior in the RTPP (Fig. 1j,k) and optical self-stimulation (Fig. 1n,o), and the optically evoked behavioral reward effect was blocked by intra-NAcc local infusion of DNQX (Fig. 1k). In addition, optogenetic activation of $CCK^{BLA\text{-}NAcc}$ or non-$CCK^{BLA\text{-}NAcc}$ glutamatergic neurons did not affect motor performance or anxiety (Extended Data Fig. 2a–g).

$CCK^{BLA\text{-}NAcc}$ and non-$CCK^{BLA\text{-}NAcc}$ glutamatergic neurons preferentially synapse with D2 and D1 subpopulations, respectively, in the NAc core. Based on the opposite emotional states mediated by BLA CCK and non-CCK neurons, we proposed that CCK and non-CCK glutamatergic neurons might activate distinct subpopulations of NAcc neurons, leading to aversion and reward. In the NAc, 95% of neurons are medium spiny neurons (MSNs), which are further divided into dopamine D1 receptor– and D2 receptor–expressing types[30].

We first employed a monosynaptic viral tracing strategy in Drd1-Cre (D1-Cre) or Drd2-Cre (D2-Cre) mice (Fig. 2a–c). Because both D1 and D2 MSNs receive monosynaptic inputs from the BLA (Extended Data Fig. 3a–h), we employed in situ hybridization to visualize BLA *Cck* mRNA expression with rabies virus–labeled $DsRed^+$ neurons from the D1-Cre or D2-Cre tracing brains (Fig. 2d,e). Interestingly, quantification revealed that the majority of $DsRed^+$ neurons in D2-Cre mice were co-localized with *Cck* mRNA, whereas few $DsRed^+$ neurons in D1-Cre mice were co-localized with *Cck* mRNA (Fig. 2f). Furthermore, employing the same labeling strategy, we collected individual $DsRed^+$ neurons from acute brain slices and performed reverse transcription PCR (RT–PCR). Results revealed that the majority (15/18) of D2 MSN–projecting BLA neurons expressed *Cck* mRNA (Extended Data Fig. 3i,j). In contrast, D1 MSN–projecting BLA neurons rarely (1/16) expressed *Cck* mRNA (Extended Data Fig. 3i,j), although *CaMKIIα* was expressed in all sampled cells in both cell populations (Extended Data Fig. 3i,k).

To confirm the anatomical results, we next used ex vivo slice physiology to characterize CCK^{BLA}-$D2^{NAcc}$ and non-CCK^{BLA}-$D1^{NAcc}$ functional connectivity. We crossed CCK-ires-Cre mice with a Drd2-GFP reporter mouse line (D2-GFP, Fig. 2g) and expressed either the 'Cre-on-ChR2' or 'Cre-out-ChR2' virus into the BLA. In situ hybridization and electrophysiological recordings showed that D2-GFP-positive neurons ($D2^+$) were mostly D2 mRNA–positive (Extended Data Fig. 4a–e) and exhibited the electrophysiological characteristics of $D2^+$ MSNs (Fig. 2h,i)[31]. We simultaneously recorded light-stimulated synaptic responses of $D2^+$ and adjacent $D2^-$ MSNs (D2-GFP-negative neurons) in NAcc brain slices. In CCK-ires-Cre::D2-GFP mice injected with the Cre-on-ChR2-mCherry virus (Fig. 2j), large optically evoked excitatory postsynaptic

Fig. 1 | NAc-projecting BLA CCK and non-CCK glutamatergic neurons encode opposite emotional valences. a,**b**, Schematic (**a**) and representative coronal images (**b**) illustrating the use of CCK-ires-Cre and Ai14-LSL-tdTomato reporter mice to label CCK-positive neurons in amygdala. Scale bar, 200 μm. **c**, Representative BLA image from a CCK-ires-Cre::Ai14 mouse stained with antibodies against GAD67, PV, SOM or CaMKIIα. Arrowheads indicate neurons labeled with one marker only, whereas arrows indicate co-labeled neurons with CCK-tdTomato. Scale bar, 40 μm. **d**, Percentage of CCK-positive neurons that co-localized with markers; $n = 10{,}584$ CCK^+ neurons from six mice. One-way ANOVA, $F_{(3,20)} = 4770$, $P < 0.0001$. **e**, Percentage of CaMKIIα-positive neurons that co-localized with CCK-tdTomato. **f**,**i**, Left, schematic of Cre-on (**f**) and Cre-out (**i**) strategies used to express ChR2(H134R) in $CCK^{BLA\text{-}NAcc}$ or non-$CCK^{BLA\text{-}NAcc}$ glutamatergic neurons. Right, representative images showing Cre-on-ChR2-mCherry (**f**) or Cre-out-ChR2-eYFP (**i**) expression in BLA and its axonal terminals in NAcc. Scale bar, 200 μm for BLA, 100 μm for NAcc. **g**,**j**, Representative tracks of real-time place avoidance (RTPA, **g**) and real-time place preference (RTPP, **j**) illustrating light-evoked behavioral aversion in Cre-on-ChR2 mice (**g**) and reward in Cre-out-ChR2 mice (**j**). **h**,**k**, Quantification of RTPA in Cre-on mice (**h**) and RTPP in Cre-out mice (**k**) and the effect of intra-NAcc pharmacological manipulations. One-way ANOVA in **h**, $F_{(4,41)} = 8.960$, $P < 0.0001$, $n = 10$ (control), 12 (ChR2), 8 (aCSF), 10 (DNQX), 6 (L-365,260) mice; One-way ANOVA in **k**, $F_{(3,32)} = 8.561$, $P = 0.0003$, $n = 8$ (control), 10 (ChR2), 10 (aCSF), 8 (DNQX) mice. Dosages were as follows: NBQX (AMPAR antagonist, 1.0 μg in 200 nl), L-365,260 (CCKA receptor antagonist, 0.1 μg in 200 nl). **l**,**n**, Left, schematic of optical activation of $CCK^{BLA\text{-}NAcc}$ neurons during sucrose positive reinforcement (**l**) and optical activation of non-$CCK^{BLA\text{-}NAcc}$ neurons during optical self stimulation (**n**). Right, number of nose pokes during baseline. Two-way ANOVA in **l**, $F_{(1,40)} = 0.1481$, $P = 0.7024$, $n = 10$, 12 mice for control and Cre-on-ChR2 groups, respectively; two-way ANOVA in **n**, $F_{(1,24)} = 1.505$, $P = 0.2318$, $n = 6$, 8 mice for control and Cre-out-ChR2 groups, respectively. **m**,**o**, Quantification of number of nose pokes during light stimulation periods in sucrose positive reinforcement (**m**) and self-stimulation (**o**). Two-way ANOVA in **m**, $F_{(1,40)} = 102.8$, $P < 0.0001$, $n = 10$, 12 for control and Cre-on-ChR2 groups, respectively. Two-way ANOVA in **o**, $F_{(1,24)} = 68.49$, $P < 0.0001$, $n = 6$, 8 mice for control and Cre-out ChR2 groups, respectively. All data are means ± s.e.m. $^{**}P < 0.01$; $^{***}P < 0.001$; $^{****} < P$ 0.0001; n.s., no significance.

currents (oEPSCs) were elicited in the majority of D2$^+$ MSNs (90%, $n=36$ out of 40), whereas only a small fraction of D2$^-$ MSNs were responsive (15%, $n=6$ out of 40, Fig. 2k) and the response was also very diminished (Fig. 2l). In comparison, in CCK-ires-Cre::D2-GFP mice injected with the Cre-out-ChR2-eYFP virus (Fig. 2n), large oEPSCs were elicited in the majority of D2$^-$ MSNs (92.5%, $n=37$ out of 40), whereas only a small fraction of D2$^+$ MSNs were responsive (12.5%, $n=5$ out of 40, Fig. 2o) and with much smaller amplitudes (Fig. 2p). We observed no differences in latency between D2$^+$and D2$^-$ cells receiving CCK or non-CCK inputs (Fig. 2m,q).

To demonstrate whether non-CCK subpopulations were connected to D1 MSNs in the NAcc, we crossed CCK-ires-Cre mice with a Drd1-tdTomato mouse line (D1-tdTomato, Extended Data Fig. 4f–h) expressing Cre-out-ChR2 virus in the BLA (Extended Data Fig. 4i). Slice experiments showed that 38 out of 40 (95%) D1-tdTomato-positive (D1$^+$) neurons received direct synaptic input

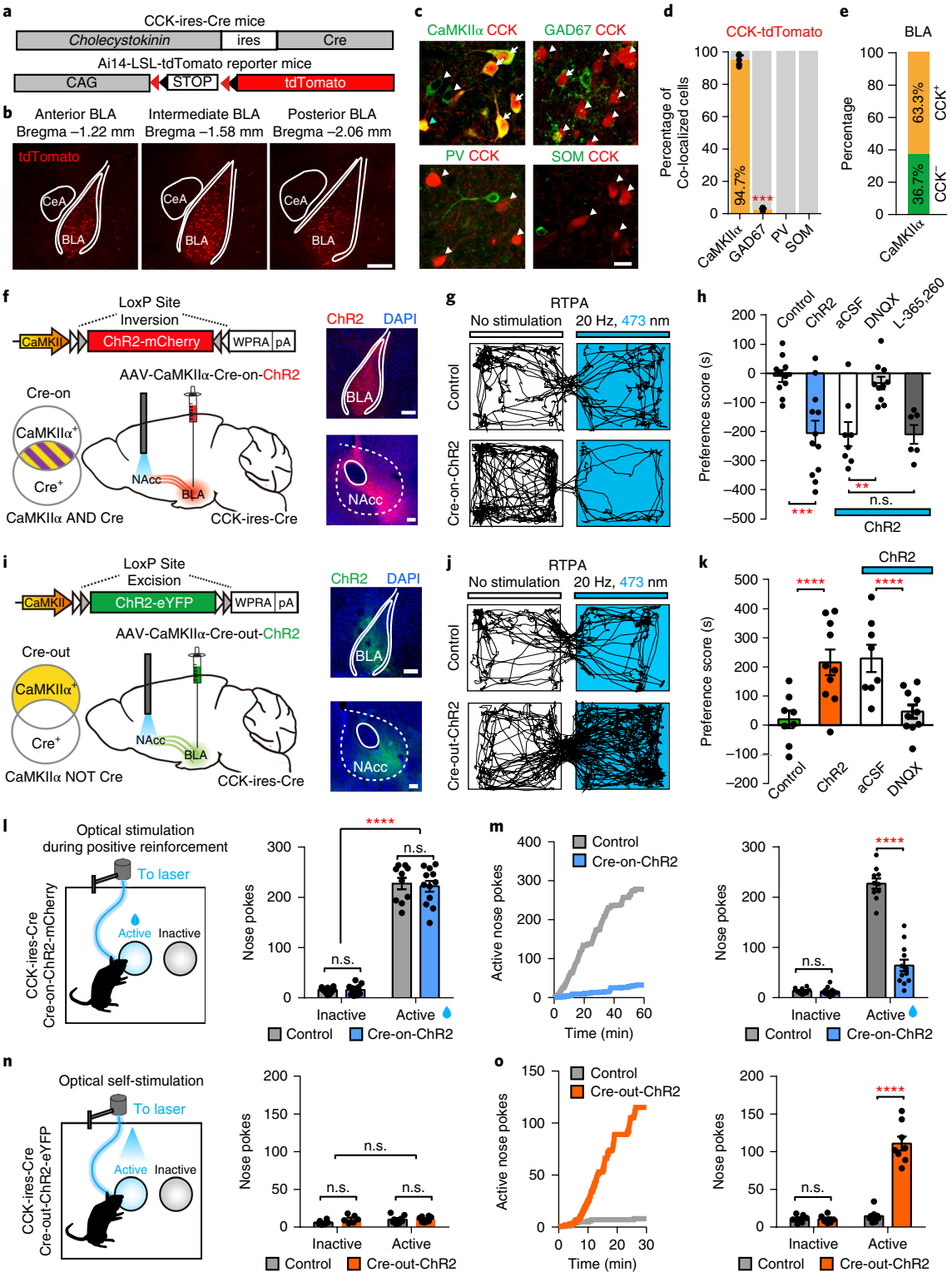

from the BLA non-CCK neurons, whereas only 6 out of 40 (15%) D1-tdTomato-negative ($D1^-$) neurons received direct synaptic input from the BLA non-CCK neurons (Extended Data Fig. 4j,k).

Collectively, these results indicate that the CCK and non-CCK glutamatergic neurons are parallel BLA-NAc circuits targeting NAcc D2 and D1 MSNs, respectively.

The CCK^{BLA}–$D2^{NAcc}$ circuit is selectively activated by social stress. Because the NAcc is strongly implicated in maladapted emotional states such as depression[32,33], we next examined whether the CCK^{BLA}–$D2^{NAcc}$ and non-CCK^{BLA}–$D1^{NAcc}$ circuits exhibited aberrant physiological adaptations in depression.

We employed a 10-day chronic social defeat stress (CSDS) -induced depression model[34] (Extended Data Fig. 5a–e). Consistent with a previous result[35], we found an increase in the frequencies of miniature EPSCs (mEPSCs) of $D2^+$ MSNs (Extended Data Fig. 5f–h) but not $D2^-$ MSNs (Extended Data Fig. 5i–k) within the NAcc of susceptible mice, suggesting that D2 MSNs play the more important role in stress susceptibility.

To detect the neuronal activity of D2 MSNs underlying social stress, we measured c-fos expression in the NAcc when D2-GFP mice were re-exposed to novel CD1 mice (Fig. 3a,b). Robust c-fos signals were detected in the NAcc of susceptible, but not of control or resilient, mice (Fig. 3c,d). Furthermore, 70.9 ± 3.1% of c-fos-positive neurons activated by stress in susceptible mice were D2 MSNs, as indicated by the D2-GFP signal (merge/c-fos, Fig. 3c,e). In addition, neurons activated by social stress accounted for 45.5 ± 3.1% of all $D2\text{-}GFP^+$ MSNs in the NAcc of susceptible mice (merge/D2 MSNs, Fig. 3c,f). These results indicate that NAcc D2 MSNs are selectively activated by social stress in susceptible mice.

We next investigated whether activation of the NAcc D2 MSNs in susceptible mice during social stress exposure was due to the recruitment of BLA CCK glutamatergic neurons. We expressed hM4Di, an inhibitory designer receptor exclusively activated by a designer receptor exclusively activated by designer drugs (DREADD), into the BLA of CCK-ires-Cre::D2-GFP mice (Fig. 3g,h). Electrophysiological analysis of acute BLA slices confirmed that clozapine-N-oxide (CNO, 5 μM) inhibited spiking in hM4Di-expressing BLA CCK neurons, resulting in a increased spike threshold and decreased spike number under the current step injection (Fig. 3i,j). G_i-DREADD inhibition of BLA CCK neurons in susceptible mice via intraperitoneal (i.p.) injection of CNO (5 mg kg^{-1}) dramatically reduced activation of NAcc D2 MSNs following stress exposure, evidenced by the decreased total c-fos number and merge/c-fos and merge/D2-GFP percentages in susceptible mice with hM4Di inhibition (Fig. 3k).

Bidirectional regulation of the CCK^{BLA}–$D2^{NAcc}$ circuit in social stress-induced depression. If heightened activity of the CCK^{BLA}–$D2^{NAcc}$ circuit is characteristic of susceptibility to social stress, we hypothesized that reducing the activity of this circuit could promote resilience to social stress. To achieve this, we expressed Arch3.0-eYFP or eYFP in BLA CCK glutamatergic neurons and selectively inhibited the CCK^{BLA}–$D2^{NAcc}$ circuit by illumination of a 537 nm yellow light into the NAcc (Fig. 4a). Light-evoked hyperpolarization was recorded in the Arch3.0-expressing BLA CCK neurons (Fig. 4b).

Previous studies have shown that chronic neural circuit-probing optogenetic manipulations reversed pathological adaptations in depressed animals[36]. We first chronically inhibited the CCK^{BLA}–$D2^{NAcc}$ circuit during a sensory period of 10 min over three consecutive days (Fig. 4c). Defeated susceptible mice receiving the eYFP virus showed a typical depressive-like phenotype (Fig. 4d–g). Interestingly, we found that defeated susceptible mice expressing Arch3.0-eYFP showed a increase in social interaction (Fig. 4d,e), as well as a dramatic improvement in the sucrose preference test (SPT, Fig. 4f) and tail-suspension test (TST, Fig. 4g). However, the same 3-day optical manipulation in non-CSDS control mice had no effect (Fig. 4d–g). These results suggest an antidepressant effect caused by 3-day chronic manipulation of the CCK^{BLA}–$D2^{NAcc}$ circuit in susceptible mice.

To further demonstrate the contribution of the CCK^{BLA}–$D2^{NAcc}$ circuit in the acquisition or expression of social avoidance, we optically inhibited the circuit during either the daily sensory contact period (encoding) or the 2.5 min social interaction task (execution). Photo-inhibition of the CCK^{BLA}–$D2^{NAcc}$ circuit during 10-day social defeat increased the proportion of resilient mice according to a validated measure of social interaction (Extended Data Fig. 6a–e) and a composite depression score (Extended Data Fig. 6f,g). Optical inhibition of the CCK^{BLA}–$D2^{NAcc}$ circuit in defeated susceptible mice also rescued social avoidance in a 2.5 min social interaction task (Extended Data Fig. 6h–j). Taken together, these results indicate that the CCK^{BLA}–$D2^{NAcc}$ circuit is critical in the neural encoding of social threat, as well as in the execution of previously established social avoidance responses.

If a decrease in the activity of the CCK^{BLA}–$D2^{NAcc}$ circuit promotes resilience, we hypothesized that artificially driving activity in this circuit could be sufficient to induce the depressive-like phenotype

Fig. 2 | BLA CCK and non-CCK glutamatergic neurons differentially form synaptic connections with D2 and D1 MSNs, respectively, in NAcc. a, Monosynaptic rabies retrograde tracing from NAcc core (NAcc) D1 MSNs in Drd1-Cre (D1-Cre) mice or D2 MSNs in Drd2-Cre (D2-Cre) mice. **b**,**c**, Left, representative image of injection sites (NAcc) in a Drd1-Cre (**b**) and a Drd2-Cre (**c**) tracing brain; scale bar, 200 μm. Right top, magnified view of left image; scale bar, 20 μm. Right bottom, quantification of co-labeled neurons showing that most starter cells are D1 (**b**, 94.3%) or D2 (**c**, 93.3%) positive. **d**, Presynaptic neurons in anterior, intermediate and posterior BLA (depending on categories of AP coordinates) from a D1-Cre tracing brain (top) and a D2-Cre tracing brain (bottom) co-labeled with *Cck* mRNA; scale bar, 200 μm. Central inset, magnified view of rectangular part; scale bar, 40 μm. **e**, Quantification of anterior–posterior distribution of presynaptic input in BLA from D1-Cre (D1-P) and D2-Cre (D2-P) tracing brains. Two-way ANOVA, $F_{(2,27)} = 0.8717$, $P = 0.4297$, $n = 5$ (D1-P), 6 (D2-P) mice. **f**, Quantification of input neurons in BLA from D1-Cre (D1-P) and D2-Cre (D2-P) tracing brains that co-labeled with *Cck* mRNA. Two-way ANOVA, $F_{(2,27)} = 5.464$, $P = 0.0102$, $n = 5$ (D1-P), 6 (D2-P) mice. **g**, Representative image of D2-GFP labeled neurons in NAcc of Drd2-GFP (D2-GFP) mice. Scale bar, 40 μm. **h**, Representative images of recorded D2–GFP positive ($D2^+$, left) and D2–GFP negative ($D2^-$, right) neurons in NAcc using in vitro slice recording. Scale bar, 20 μm. **i**, Representative traces (left) of whole-cell current-clamp recordings from $D2^+$ ($n = 12$ neurons from 3 mice) or $D2^-$ ($n = 12$ neurons from 3 mice) MSNs in vitro and current-voltage (I-V) curves (right) of $D2^+$ and $D2^-$ MSNs. Raw traces show individual voltage responses to a series of 600-ms current pulses from −300 pA to 300 pA with 200-pA steps. **j**,**n**, Schematic showing tested connections. In CCK-ires-Cre::D2-GFP mice, CCK neurons were transduced by an injection of AAV-CaMKIIα-Cre-on-ChR2-mCherry in BLA (**j**), and non-CCK neurons were transduced by an injection of AAV-CaMKIIα-Cre-out-ChR2-eYFP in BLA (**n**). **k**,**o**, Left, light responses recorded from two adjacent $D2^+$ or $D2^-$ MSNs following 5-ms laser stimulation of ChR2-expressing CCK (**k**) or non-CCK (**o**) terminals from BLA. Right, connectivity charts are shown. **l**,**m**,**p**,**q**, Quantification of amplitude (**l**,**p**) and latency (**m**,**q**) of oEPSCs recorded in NAcc $D2^+$ MSNs and $D2^-$ MSNs from either BLA CCK or non-CCK glutamatergic neurons. Two-sided unpaired *t*-test in (**l**,**m**,**p**,**q**); $t = 9.798$, d.f. = 40, $P < 0.0001$ in **l**, $t = 0.03074$, d.f. = 40, $P = 0.9756$ in **m**, $n = 36$ out of 40 $D2^+$ MSNs (90%) and 6 out of 40 $D2^-$ MSNs (15%) from 6 mice; $t = 5.822$, d.f. = 40, $P < 0.0001$ in **p**, $t = 0.05795$, d.f. = 40, $P = 0.9541$ in **q**, $n = 5$ out of 40 $D2^+$ MSNs (12.5%) and 37 out of 40 D2-MSNs (92.5%) from 6 mice. All data are means ± s.e.m. $^*P < 0.05$; $^{**}P < 0.01$; $^{****}P < 0.0001$; n.s., no significance.

in a two-trial subthreshold social defeat stress (SSDS) paradigm. To test this, we selectively expressed ChR2-mCherry in BLA CCK neurons and inserted an optical fiber into the NAcc (Fig. 4h). Action potential was evoked by 5 ms blue light stimulation in ChR2-expressing BLA CCK neurons (Fig. 4i). BLA-NAc neurons show a physiological firing rate that ranges from 0 to 10 Hz in awake and behaving mice[37]. In addition, 20 Hz stimulation of the CCK^{BLA}–$D2^{NAcc}$ circuit was sufficient to induce behavioral aversion in RTPA (Fig. 1f–h). Thus, we chose a 1 Hz (physiological) and 20 Hz (pathological) stimulation pattern to activate the CCK^{BLA}–$D2^{NAcc}$ circuit (Fig. 4j). We found that 20 Hz priming pulses of blue light induced stress susceptibility in the social interaction test (Fig. 4k,l), decreased

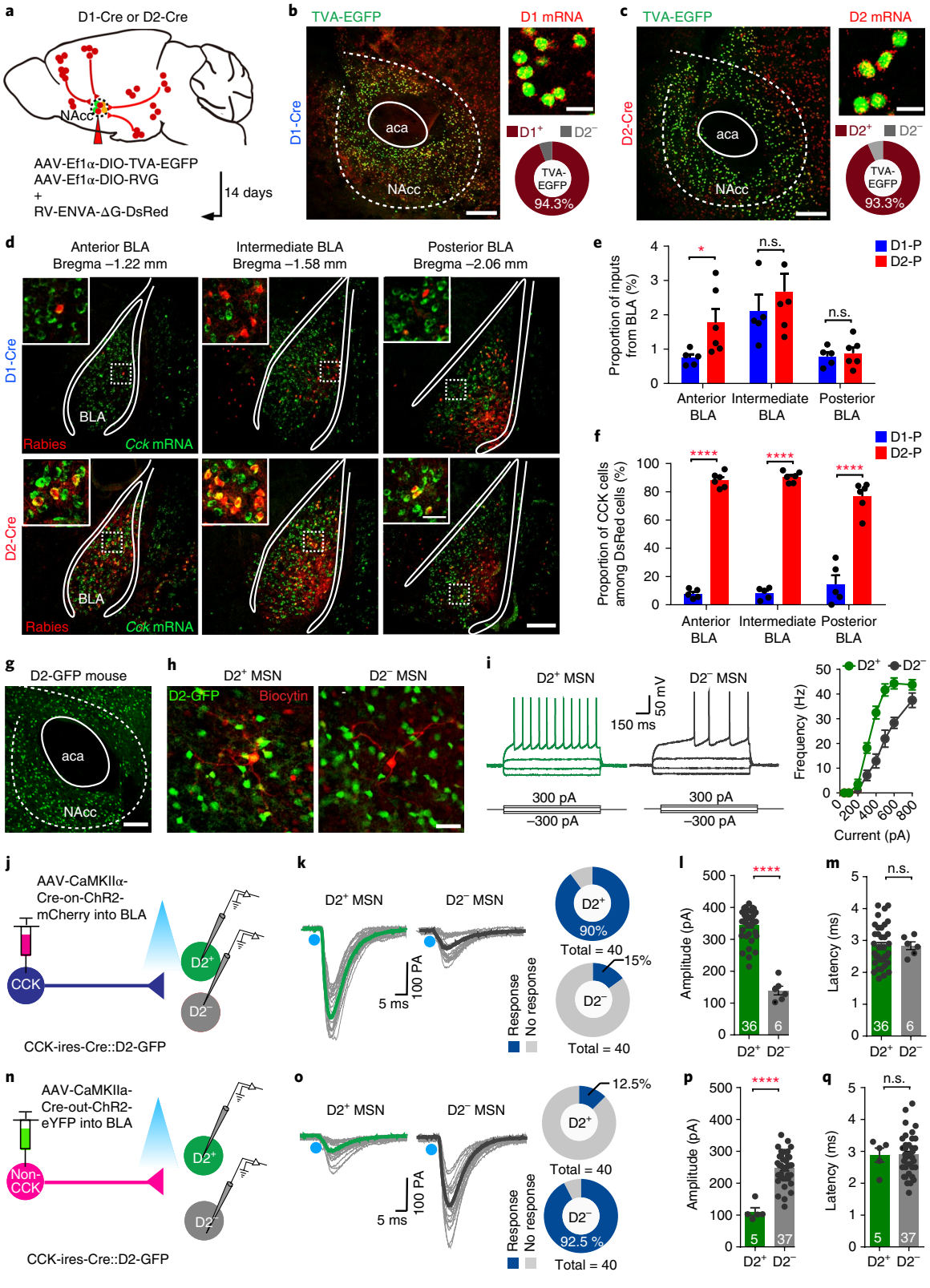

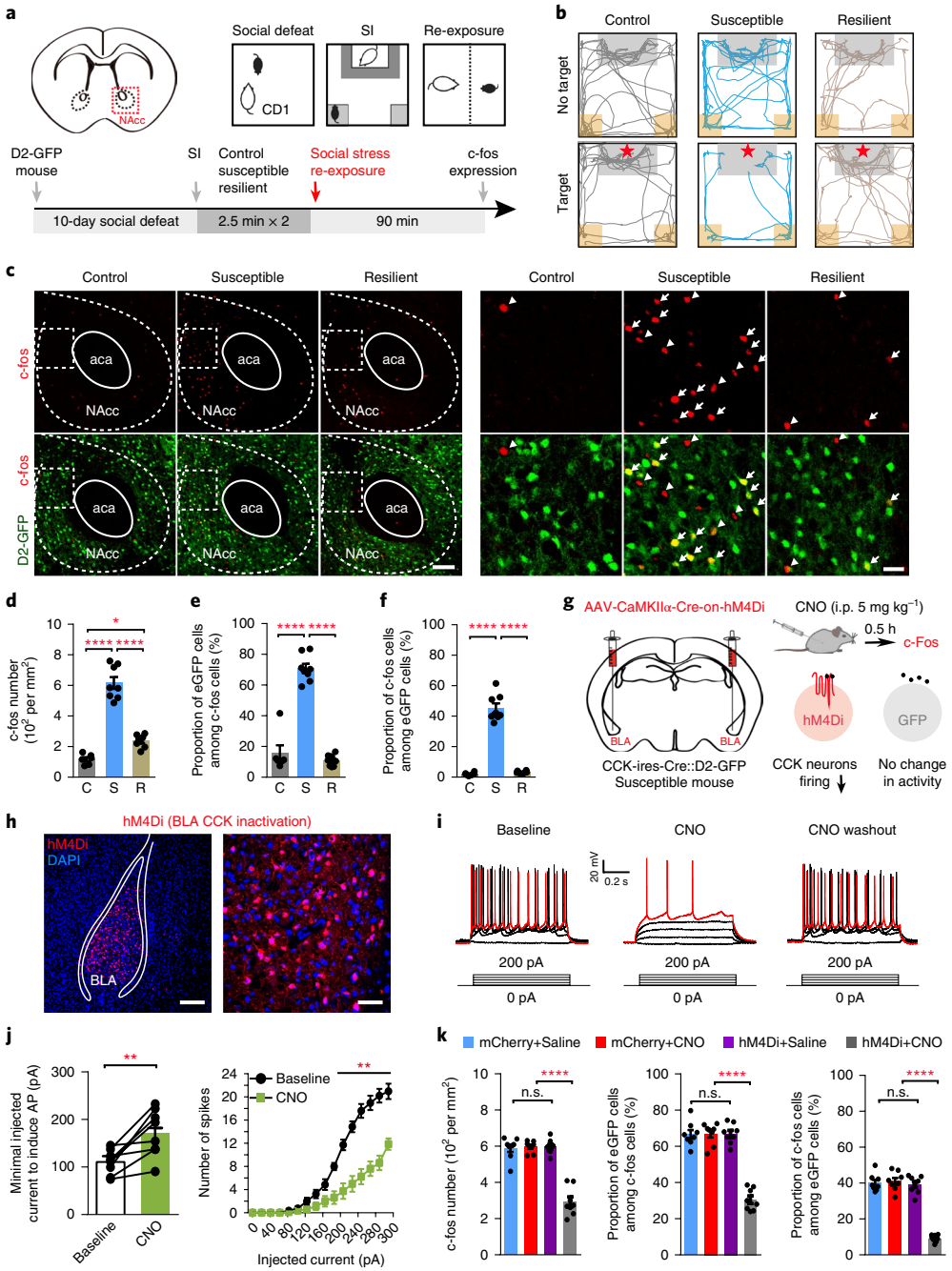

Fig. 3 | Social stress activates CCK^{BLA}–D2^{NAcc} circuit in susceptible mice. a, Schematic (top) and workflow (bottom) of c-fos experimental design. C-fos expression was specifically tested in NAcc, marked by the red rectangle. **b**, Representative traces in absence (top) and presence (bottom) of a social target in the social interaction (SI) test. The red star indicates the social target. **c**, Left, c-fos expression (top) and co-labeled with D2-GFP (bottom) in NAcc; scale bar, 100 μm. Right, magnified view of left image indicated in white rectangle. Arrowheads indicate neurons labeled with c-fos only, whereas arrows indicate neurons co-labeled with D2-GFP; scale bar, 25 μm. **d**–**f**, Quantification of c-fos number (**d**), proportion of c-fos-positive cells that co-express D2-GFP (**e**) and proportion of D2-GFP-positive cells that co-express c-fos (**f**) in control (C), susceptible (S) and resilient (R) groups. One-way ANOVA in **d**–**f**. $F_{(2,19)} = 94.14$, $P < 0.0001$ in **d**. $F_{(2,19)} = 112.7$, $P < 0.0001$ in **e**. $F_{(2,19)} = 162.5$, $P < 0.0001$ in **f**. $n = 6$ (control), 8 (susceptible), 8 (resilient) mice in **d**–**f**. **g**, Stereotaxic infusion of AAV-CaMKIIα-Cre-on-hM4Di-mCherry virus into BLA of CCK-ires-Cre::D2-GFP mice with i.p. injection of CNO (5 mg kg^{-1}) to inhibit neural activity. **h**, Left, hM4Di expression in BLA; scale bar, 200 μm. Right, magnified image; scale bar, 50 μm. **i**, Current–voltage relationship of a representative BLA CCK neuron recorded before, during and after CNO perfusion (5 μM). Raw traces show individual voltage responses to a series of 600 ms current pulses from 0 to 200 pA in 20 pA steps. Red traces indicate number of 200 pA current-induced action potentials. **j**, Left, minimal injected current to induce action potentials (APs) was increased by CNO (5 μM) administration. Two-sided paired *t*-test, $t = 3.968$, d.f. = 7, $P = 0.0054$. Right, number of induced APs at different current steps, two-sided paired *t*-test, $t = 3.858$, d.f. = 7, $P = 0.0015$. $n = 8$ neurons from 3 mice. **k**, Quantification of c-fos number in NAcc (left), proportion of c-fos-positive cells that coexpress D2-GFP (middle) and proportion of D2-GFP-positive cells that coexpress c-fos (right) in susceptible mice expressing either mCherry or hM4Di virus in BLA CCK neurons with i.p. injection of saline or CNO (5 mg per kg). One-way ANOVA in **k**: left, $F_{(3,28)} = 59.51$, $P < 0.0001$; middle, $F_{(3,28)} = 71.80$, $P < 0.0001$; right, $F_{(3,28)} = 99.21$, $P < 0.0001$. $n = 8$ mice for each group. All data are means ± s.e.m. *$P < 0.05$; ****$P < 0.0001$; n.s., no significance.

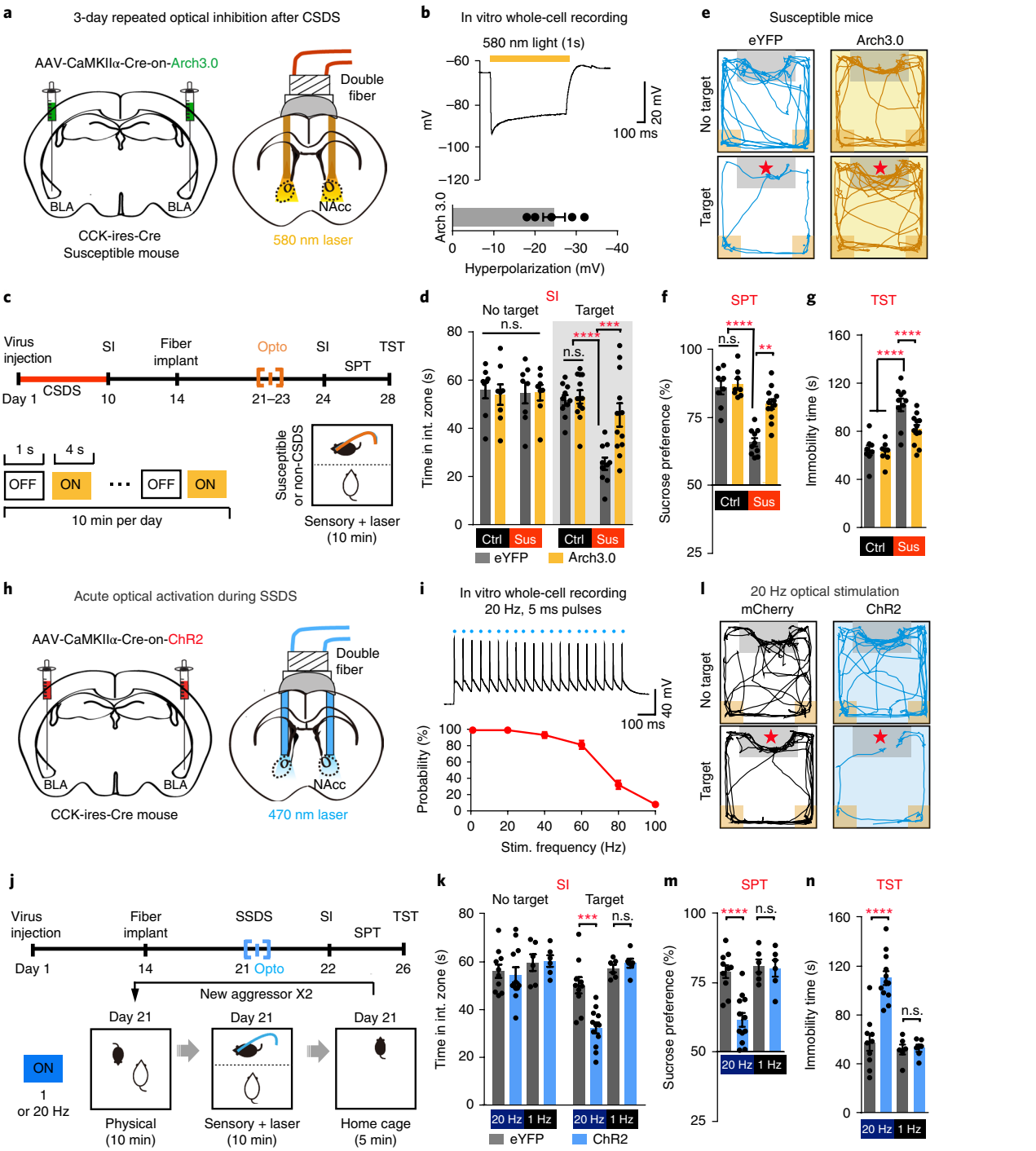

Fig. 4 | Optogenetic inhibition or activation of CCK^{BLA}–D2^{NAcc} circuit bidirectionally regulates susceptibility to social stress. a,**h**, Schematic of virus injection to express Arch3.0 (**a**) or ChR2 (H134R) (**h**) in CCK$^{BLA\text{-}NAcc}$ glutamatergic neurons and optical fiber implantation in NAcc. **b**,**i**, Representative voltage-clamp traces (**b**, top) or current-clamp traces (**i**, top) from in vitro slice recordings of a BLA Arch3.0-expressing (**b**) or ChR2-expressing (**i**) neurons illuminated by 1 s yellow light stimulation (**b**) or 20 Hz blue light stimulation (**i**). Summary plot (**b**, bottom) showing light-evoked robust hyperpolarization (average 24.6 mV); $n = 5$ neurons from 3 mice. Plot (**i**, bottom) of spike probability versus stimulation frequency showing that photostimulation reliably triggered action potentials to each 141 pulse in 20 Hz; $n = 5$ neurons from 3 mice. **c**,**j**, Paradigms of 3-day repeated optical inhibition of the CCK^{BLA}–D2^{NAcc} circuit in susceptible mice following 10-day chronic social defeat stress (CSDS) and in non-CSDS control mice (**c**), and 1 Hz and 20 Hz phasic activation of the CCK^{BLA}–D2^{NAcc} circuit during social interaction in a two-trial subthreshold social defeat stress (SSDS) paradigm (**j**). Top, experimental timeline. Bottom, detailed schematic. **d**,**k**, Social interaction time in absence or presence of social target. Two-way ANOVA in **d**, $F_{(3,34)} = 147\ 4580$, $P = 0.0085$. Two-way ANOVA in **k**, $F_{(3,30)} = 9.752$, $P < 0.0001$. **e**,**l**, Representative tracks of eYFP and Arch3.0 group following 3-day yellow light repeated stimulation treatment in susceptible mice (**e**) or of mCherry and ChR2 group following 20 Hz phasic blue light stimulation during two-trial SSDS (**l**) in either the absence (top) or presence (bottom) of a social target. **f**,**m**, Sucrose preference in sucrose preference test (SPT). One-way ANOVA in **f**, $F_{(3,34)} = 18.23$, $P < 0.0001$. One-way ANOVA in **m**, $F_{(3,30)} = 15.03$, $P < 0.0001$. **g**,**n**, Total immobility time in tail-suspension test (TST). One-way ANOVA in **g**, $F_{(3,34)} = 26.20$, $P < 0.0001$. One-way ANOVA in **n**, $F_{(3,30)} = 26.95$, $P < 0.0001$. All data are means ± s.e.m. $^{**}P < 0.01$;*** $P < 0.001$; **** $P < 0.0001$; n.s., no significance.

performance in the SPT (Fig. 4m) and increased immobility in the TST (Fig. 4n). In contrast, 1 Hz stimulation had no effect (Fig. 4k,m,n). Furthermore, chemogenetic inactivation (Extended Data Fig. 7a–e) and activation (Extended Data Fig. 7f–m) of the CCK^{BLA}–$D2^{NAcc}$ circuit replicated these optogenetic effects.

Downregulation of CB_1R mediates increased synaptic activity in the CCK^{BLA}–$D2^{NAcc}$ circuit of susceptible mice. To understand the underlying mechanisms mediating elevated activity in the CCK^{BLA}–$D2^{NAcc}$ circuit of susceptible mice, we first examined synaptic transmission by determining the input–output relationship between optical stimulation intensity and BLA CCK oEPSC amplitude in D2 MSNs (Fig. 5a,b). Susceptible mice displayed increased BLA CCK oEPSC amplitudes at higher stimulation intensities (Fig. 5c). In addition, a decrease in the paired-pulse ratio (PPR, Fig. 5d) and absence of changes in the AMPAR/NMDAR (A/N) amplitude ratio (Fig. 5e) indicated that increased synaptic efficacy in susceptible mice was a consequence of increased probability of presynaptic release, rather than a change in postsynaptic strength. No changes in the intrinsic activity of BLA CCK neurons (Fig. 5f,g) were detected in susceptible mice.

Given that presynaptic CB_1R mediate presynaptic inhibition[38–40] and are co-expressed with CCK in several areas of the brain[28,41,42], we tested whether CB_1R are expressed in the CCK^{BLA}–$D2^{NAcc}$ circuit. Results from double-labeling in situ hybridization of *Cck* and *Cb$_1$r* mRNA (Fig. 5h) showed that 92.7% of *Cb$_1$r*-mRNA-positive neurons in the BLA overlapped with *Cck* mRNA and 84.1% of *Cck* mRNA–positive neurons overlapped with *Cb$_1$r* mRNA (Fig. 5i), suggesting that *Cck* and *Cb$_1$r* are highly co-localized in the BLA. Using rabies tracing–aided single-cell RT–PCR, we showed that *Cb$_1$r* mRNA was selectively expressed in D2-projecting BLA CCK neurons but not in D1-projecting BLA non-CCK neurons (Extended Data Fig. 3i,l). Furthermore, application of the CB_1R agonist WIN55,212-2 reduced the amplitude of oEPSCs and simultaneously increased the PPR in control mice (Fig. 5j–l). In contrast, oEPSCs evoked in the non-CCK^{BLA}–$D1^{NAcc}$ circuit were insensitive to WIN55,212-2, confirming the absence of CB_1R on BLA non-CCK terminals (Extended Data Fig. 8a–c).

On the basis of increased synaptic activity in the CCK^{BLA}–$D2^{NAcc}$ circuits of susceptible mice and the notion that CB_1R within this circuit regulates synaptic transmission, we predicted that CB_1R in this circuit is related to stress susceptibility. Western blot analysis showed that CB_1R expression levels in the NAcc of susceptible mice were lower than those in the NAcc of resilient or control mice (Fig. 5m and Source Data Fig. 1). In contrast, levels of several other synaptic proteins did not change (Fig. 5m). Notably, there was a correlation between the level of CB_1R in the NAcc and the social interaction ratio (Fig. 5n).

Next, we determined whether CB_1R modulation of the CCK^{BLA}–$D2^{NAcc}$ oEPSCs differed owing to the reduction in CB_1R. We found that WIN55,212-2 (1 μM,10 min) decreased oEPSC amplitude to approximately 49.77% and 51.78% of the baseline in control and resilient mice, respectively. However, in susceptible mice, WIN55,212-2 reduced the oEPSC amplitude to only 79.39% (Fig. 5o). To confirm in vivo that CB_1R-mediated synaptic inhibition was reduced in susceptible mice, we recorded optically evoked field excitatory postsynaptic potentials (oEPSPs) to measure the BLA-NAc synaptic efficacy (Fig. 5p and Extended Data Fig. 9a–d). oEPSPs from BLA CCK to NAcc synapses in anesthetized control and resilient mice revealed that an i.p. injection of HU210 (0.05 mg kg^{-1}), a potent synthetic cannabinoid, decreased the oEPSP slopes to approximately 39.1% and 44.5% of baseline levels, respectively. However, in susceptible mice, HU210 reduced the oEPSP slope to only 77.2% (Fig. 5q and Extended Data Fig. 9e).

Modulation of CB_1R in the CCK^{BLA}–$D2^{NAc}$ circuit regulates stress susceptibility. To investigate whether changes in CB_1R levels at CCK^{BLA}–$D2^{NAcc}$ synapses are crucial to both synaptic functions and stress susceptibility, we selectively knocked down CB_1R in mice (CB_1-KD mice) at the CCK^{BLA}–$D2^{NAcc}$ circuit using the Cre-dependent short-hairpin (sh) CB_1R virus and observed that CB_1R were effectively deleted in the BLA on the side of virus injection, as revealed by decreased *Cb$_1$r* mRNA expression (Fig. 6a,b). Western blot analysis of the NAcc confirmed the reduction in CB_1R protein expression in CB_1-KD mice (Fig. 6c and Source data Fig. 2). To investigate the functional disruption of CB_1R, we included the CaMKIIα-Cre-on-ChR2-mCherry virus in some BLA injections (Fig. 6d) and found that WIN55,2212-2 did not obviously reduce CCK^{BLA}–$D2^{NAcc}$ oEPSCs in virally injected

Fig. 5 | Reduced CB_1 levels lead to increased synaptic activity in CCK^{BLA}-$D2^{NAcc}$ circuit of susceptible mice. a, Schematic of virus injection to express ChR2 in BLA of CCK-ires-Cre::D2-GFP mice and in vitro slice recording in D2-GFP-positive neurons in NAcc. **b**, Representative traces of oEPSC amplitude in response to graded optical stimulation (1, 5, 10, 15, 20 mW) (top), 50 ms PPR (middle) and intrinsic excitability (bottom) of BLA CCK neurons. **c**, Susceptible mice displayed increased BLA CCK oEPSCs amplitude relative to control and resilient mice under higher stimulation intensity. Two-way ANOVA, $F_{(8, 116)} = 3.504$, $P = 0.0012$, $n = 10$ (control), 12 (susceptible), 10 (resilient) neurons, each from 6 mice. **d**,**e**, 50 ms PPR (**d**) of BLA CCK oEPSC decreased in susceptible mice, whereas A/N ratio (**e**) of BLA CCK oEPSCs was not different between groups. One-way ANOVA in **d**, $F_{(2, 29)} = 5.226$, $P = 0.0115$, $n = 10$ (control), 12 (susceptible), 10 (resilient) neurons, each from 6 mice. One-way ANOVA in **e**, $F(2, 15) = 0.1069$, $P = 0.8993$, $n = 6$ neurons for each group, each from 3 mice. **f**,**g**, Resting membrane potential (RMP) (**f**) and minimal voltage threshold to induce APs (**g**) were not different between groups. One-way ANOVA in **f**, $F_{(2, 15)} = 0.1051$, $P = 0.9009$. One-way ANOVA in **g**, $F_{(2, 15)} = 0.1718$, $P = 0.8438$. $n = 6$ neurons for each group, each from 3 mice. **h**, Left, representative image of *Cck* mRNA and *Cb$_1$* mRNA expression in BLA of a wild-type mouse; scale bar, 200 μm. Right, a magnified view; scale bar, 10 μm. **i**, Left, percentage of *Cb$_1$* mRNA–positive neurons that coexpress CCK. Right, percentage of *Cck* mRNA–positive neurons that coexpress *Cb$_1$* mRNA. $n = 1{,}555$ neurons from 5 mice. **j**, Schematic of in vitro slice recording to testing expression of CB_1R in CCK^{BLA}–$D2^{NAcc}$ circuit. **k**, Left, normalized oEPSC following application of CB_1 agonist WIN55,212-2 (10 min, 1 μM). Right, representative traces of oEPSC (top) and 50 ms PPR (bottom) in absence (left) and presence (right) of WIN55,212-2 (10 min, 1 μM). $n = 6$ neurons from 3 mice. **l**, Relative (normalized to baseline) oEPSC amplitude (left) and PPR (right) following WIN55,212-2 application (10 min, 1 μM). Two-sided paired *t*-test for amplitude, $t = 8.685$, d.f. = 5, $P = 0.0003$. Two-sided paired *t*-test in PPR, $t = 2.726$, d.f. = 5, $P = 0.0415$. $n = 6$ neurons from 3 mice. **m**, Western blot image (left) and quantification (right) of CB_1, Cav2.1, SNAP25, RIMS 3 and GAPDH levels in NAcc. The blots are cropped according to their molecular weight. Tissue level of GAPDH was used as loading control. Protein expression was normalized by the control level. One-way ANOVA, $F_{(2, 29)} = 13.44$, $P < 0.0001$, $n = 16$ (control), 14 (susceptible), 12 (resilient) mice in CB_1, $n = 8$ (control), 8 (susceptible), 6 (resilient) mice in Cav2.1, SNAP25 and RIMS3. **n**, Relationship between CB_1 level in NAcc and SI (Pearson correlation), $n = 7$ mice for each group. $r^2 = 0.5610$, $P = 0.0001$. **o**, Relative amplitude (percentage normalized to baseline) of BLA CCK oEPSC following WIN55,212-2 application (10 min, 1 μM). One-way ANOVA, $F_{(2, 19)} = 9.932$, $P = 0.0011$, $n = 6$, 8, 8 neurons from 3, 4, 4 mice for control, susceptible and resilient groups, respectively. **p**, Schematic of in vivo fEPSPs recordings in anesthetized mice. **q**, Plots of normalized fEPSP slopes (left) following HU210 i.p. injection, and statistics (right) for normalized fEPSP slopes. One-way ANOVA, $F_{(2, 10)} = 17.24$, $P = 0.0006$, $n = 3$ (control), 5 (susceptible), 5 (resilient) mice. All data are means ± s.e.m. $^*P < 0.05$; $^{**}P < 0.01$; $^{***}P < 0.001$; $^{****}P < 0.0001$; n.s., no significance.

CB_1-KD mice (Fig. 6e). Furthermore, i.p. injection of HU210 decreased the oEPSP slope in control mice but not in CB_1-KD mice (Fig. 6f and Extended Data Fig. 9f). Together, these results indicate the functional disruption of CB_1R in the CCK^{BLA}–$D2^{NAcc}$ circuit of CB_1-KD mice.

We further examined whether CB_1R knockdown in the CCK^{BLA}–$D2^{NAcc}$ circuit influenced both synaptic transmission and stress susceptibility. We found an increased input–output relationship and reduced 50 ms PPR in the CCK^{BLA}–$D2^{NAc}$ oEPSCs of CB_1-KD mice (Fig. 6g), mimicking the synaptic changes occurring in susceptible mice. To assess stress susceptibility, we adopted a 3-day SSDS[43] (Fig. 6h). Baseline social interactions of CB_1-KD mice were similar to those of the scrambled controls (Fig. 6i). Notably, following 3-day SSDS, the CB_1-KD mice spent less time in the interaction zone than the controls (Fig. 6i). In addition, CB_1-KD mice also displayed reduced sucrose preference in the SPT (Fig. 6j) and

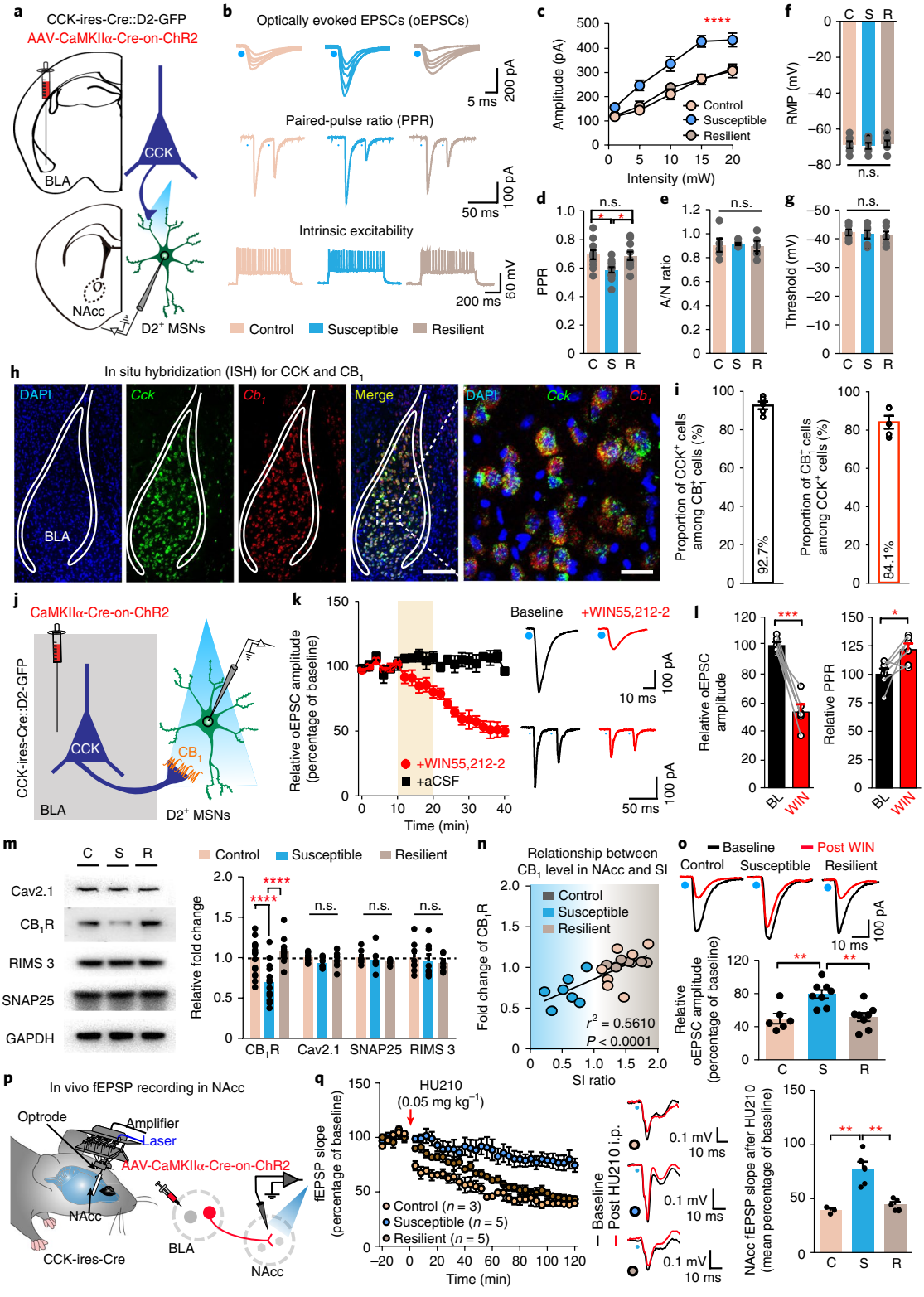

increased immobility time in the TST (Fig. 6k). Because shRNA can have off-target effects, we also attempted a pharmacological approach by repeatedly infusing CB_1R antagonist AM251 (1 μg in 100 nl each side) bilaterally into the NAcc, which also induced a susceptible phenotype (Extended Data Fig. 8d–g). These data established that CB_1R expressed in the CCK^{BLA}–$D2^{NAcc}$ circuit are required for resilience to social stress.

In contrast, to determine whether activation of residual CB_1R can reverse depressive-like symptoms, we performed a 3-day repeated intra-NAcc local infusion of CB_1R agonist WIN55,212-2 (0.5 μg in 100 nl each side) in susceptible mice following 10-day CSDS (Fig. 6l and Extended Data Fig. 9g). This manipulation resulted in strong antidepressant effects, reversing social avoidance (Fig. 6m) as well as improving performance in the SPT (Fig. 6n) and TST (Fig. 6o). This 3-day local infusion of WIN55,212-2 repeated in resilient mice did not influence performance in the social interaction, SPT or TST (Extended Data Fig. 8h–k). Modulation of CB_1R in NAcc did not affect anxiety-related behavior (Extended Data Fig. 10a–i). Consistent with our previous results demonstrating that CCK glutamatergic neurons do not project into the NAc medial shell (Extended Data Fig. 1c,d), infusion of WIN55,212-2 into this structure did not rescue the depressive-like phenotype (Fig. 6l–o). The above results suggest that activation of CB_1R by cannabinoids within the CCK^{BLA}–$D2^{NAcc}$ circuit results in antidepressant effects.

Discussion

Through the use of immunohistochemistry, viral tracing and ex vivo electrophysiology, we found that the CCK neuropeptidergic neurons in the BLA were predominantly glutamatergic, long-projecting and excitatory, selectively targeting D2 MSNs in the NAcc. Optogenetic manipulation of the CCK^{BLA}–$D2^{NAcc}$ circuit drives negative behavior and disrupts positive reinforcement. One recent study showed that the $CCK^{NTS\text{-}PVH}$ pathway mediates satiating function by encoding positive valence[44]. Together, these findings add to the growing evidence of the involvement of CCK neuropeptidergic neurons in valence encoding.

Interestingly, our experiments indicated that social stress selectively activates the CCK^{BLA}–$D2^{NAcc}$ circuit. This is consistent with previous studies demonstrating that stress activates neuronal subpopulations expressing *Cck* in the medial amygdala[45] and that NAcc D2 MSNs underlie stress susceptibility[46]. Of note, we found that inhibiting BLA CCK neuronal outputs to the NAcc in susceptible mice ameliorated depressive-like behavior. These results suggest that endogenous activity of the CCK^{BLA}–$D2^{NAcc}$ circuit in susceptible male mice conveys information related to stress susceptibility. However, whether CCK neuropeptidergic neurons are generally involved in stress processing in other neural circuits, or in female mice, awaits further investigation.

Recent studies have reported that Rspo2 (R-spondin 2)- and Ppp1r1b (protein phosphatase 1 regulatory inhibitor subunit 1B)-expressing excitatory neurons in the BLA participate in aversion and reward behavior, respectively[13,47]. Triple-labeled in situ hybridization of *Cck*, *Rspo2* and *Ppp1r1b* mRNA revealed that *Cck* mRNA–positive neurons showed extensive co-localization with *Rspo2* but not with *Ppp1r1b* (Extended Data Fig. 2h,i), suggesting that *Cck* and *Rspo2* may uniquely label the same subpopulations encoding negative emotions in the BLA.

Previous results have shown that CB_1Rs are selectively expressed in the presynapses targeting D2 MSNs[48,49]. However, whether CB_1Rs are also located in the BLA afferent to the NAcc is unclear. Here we demonstrated that CB_1Rs are selectively expressed at the CCK^{BLA}–$D2^{NAcc}$ circuit and described a synaptic framework wherein circuit-specific CB_1R modulation of glutamatergic transmission shapes the information flow from BLA to the NAcc.

CB_1R-knockout mice exhibit increased corticosterone levels[15] and display depressive-like symptoms[16–19]. These findings suggest that deficiency in CB_1R represents an important substrate for depression[50–52]. However, the circuitry crucial for this CB_1R-dependent regulation is unknown. Here we demonstrated that CB_1R levels at the CCK^{BLA}–$D2^{NAcc}$ circuit were reduced in susceptible mice and that selective knockdown of CB_1R within this circuit was sufficient to promote stress susceptibility. Whether the reduction of CB_1R in the NAc can be used as a biomarker for MDD diagnosis needs to be further determined by evaluation of CB_1R levels in the NAcc of patients with major depression.

What causes CB_1R reduction at the CCK^{BLA}–$D2^{NAcc}$ synapses in susceptible mice? Ventral tegmental area dopamine neurons have been shown to increase firing in susceptible mice[36,53]. Dopamine is hypothesized to act primarily at D2 receptors to activate presynaptic

Fig. 6 | Loss- or gain-of-function of CB1 Receptors at CCK^{BLA}–$D2^{NAcc}$ synapses causes or rescues depression-like behaviors. a, Schematic of Cre-dependent AAV vectors for expressing miR30-shCB1R-eGFP. **b**, AAV-CaMKIIα-DIO-miR30-shCB1R-eGFP (green) was unilaterally injected into BLA of CCK-ires-Cre mice, and co-immunostained for Cb_1 mRNA. Representative image (top) and statistical comparison of number of Cb_1 mRNA-positive neurons in BLA and VMH between virus injection side (AAV^+) and non-virus-injection side (AAV^-) . Scale bar, 1 mm. Two-sided paired *t* test in BLA, $t = 11.49$, d.f. = 5, $P < 0.0001$, $n = 6$ mice. Two-sided paired *t*-test in VMH, $t = 0.3030$, d.f. = 5, $P = 0.7741$, $n = 6$ mice. **c**, Western blot representation (top) and quantification (bottom) of CB_1R in NAcc between groups; the blots are cropped according to their molecular weight. Two-sided unpaired *t*-test, $t = 7.516$, d.f. = 10, $P < 0.0001$, $n = 6$ mice for each group. **d**, Schematic (left) of co-expression of ChR2-mCherry and mi30-shCB$_1$R-eGFP in BLA of CCK-ires-Cre:: D2-GFP mice, with whole-cell in vitro recording of NAcc D2-GFP-positive neurons. Representative image (middle) and percentage of mCherry-positive neurons that co-express mi30-shCB1R-eGFP (right). Scale bar, 200 μm. **e**, Representative traces (left) and relative amplitude (right, % normalized to baseline) of BLA CCK oEPSC following application of WIN55,212-2 (10 min, 1 μM). Two-sided unpaired *t*-test, $t = 4.083$, d.f. = 5, $P = 0.0004$, $n = 6$ neurons from 3 mice. **f**, Left, plots of normalized fEPSPs slopes in anesthetized mice following HU210 i.p. injection. Right, statistics for normalized fEPSP slopes. Two-sided unpaired *t*-test, $t = 4.671$, d.f. = 7, $P = 0.0023$, $n = 5$ (control), 4 (CB_1-KD) mice. **g**, Representative traces (top) and quantification (bottom) of BLA CCK oEPSC amplitude (left) in response to graded optical stimulation (1, 5, 10, 15, 20 mW) and 50 ms PPR (right). Two-way ANOVA of amplitude, $F_{(4, 64)} = 9.437$, $P < 0.0001$. Two-sided unpaired *t*-test in PPR, $t = 4.125$, d.f. = 16, $P = 0.0008$. $n = 8$ (control), 10 (CB_1-KD) neurons, each from 5 mice. **h**, Schematic of 3-day sub-threshold social defeat stress (SSDS) protocol. **i,** Social interaction test. Left, time spent in interaction zone by non-defeated mice; two-way ANOVA, $F_{(1,32)} = 0.08546$, $P = 0.7719$. Right, social interaction test for defeated mice, with time spent in interaction zone shown; two-way ANOVA, $F_{(1,32)} = 36.32$, $P < 0.0001$. $n = 8$, 10 mice for control and CB_1-KD groups, respectively. **j**,**k**, Sucrose preference in SPT (**j**) and total immobility time in TST (**k**) after 3-day SSDS. Two-sided unpaired *t*-test in (**j**), $t = 4.507$, d.f. = 18, $P = 0.0003$, $n = 8$, 12 mice for control and CB_1-KD groups, respectively. Two-sided unpaired *t*-test in **k**; $t = 4.166$, d.f. = 18, $P = 0.0006$, $n = 8$, 12 mice for control and CB_1-KD groups, respectively. **l**, Infusion sites of drugs verified by 100 nl of CTB-555 in NAc core (NAcc, left) or by 100 nl CTB-488 in NAc medial shell (MNAcsh, right); scale bar, 200 μm. **m**–**o**, Effects of local bilateral infusion of WIN55,212-2 (0.5 μg, 100 μl each side) into NAcc or MNAc shell on social interaction time (**m**), SPT (**n**) and TST (**o**). Two-way ANOVA in **m**, $F_{(1,36)} = 48.09$, $P < 0.0001$. One-way ANOVA in **n**, $F_{(3,30)} = 7.333$, $P = 0.0008$. One-way ANOVA in **o**, $F_{(3,30)} = 14.24$, $P < 0.0001$. $n = 6$ (vehicle (NAcc)), 14 (WIN (NAcc)), 6 (vehicle (MNAcsh)), 8 (WIN (MNAcsh)) mice for each group. All data are means ± s.e.m. $^{**}P < 0.01$; $^{***}P < 0.001$; $^{****}P < 0.0001$; n.s., no significance.

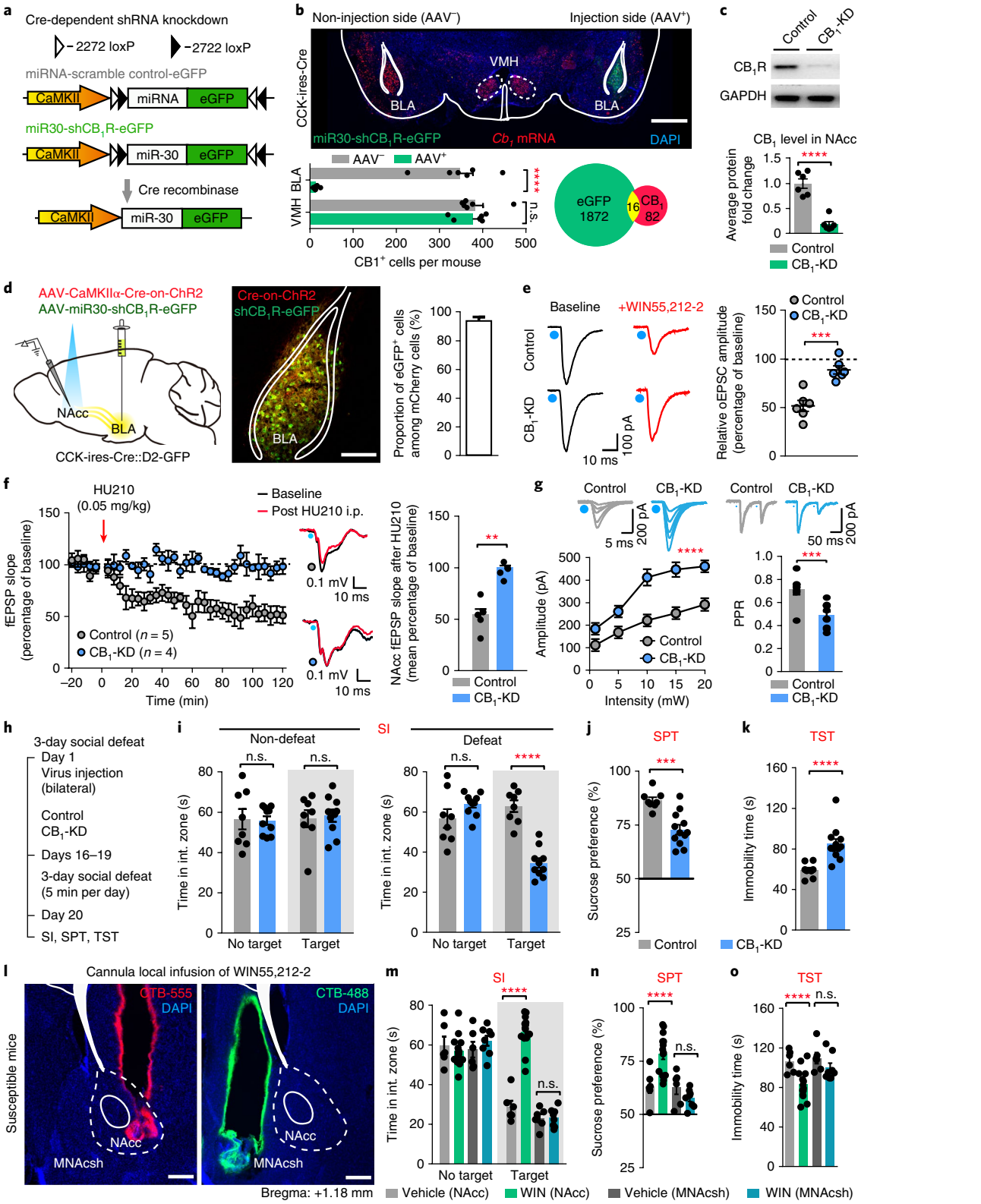

CB_1R[54,55]. Thus, increased DA neuron activity may lead to sustained activation of CB_1R, resulting in adaptation through internalization of CB_1R at the synapses. However, the detailed mechanisms need to be further studied.

Together, our findings demonstrate a critical role for CB_1R in the regulation of synaptic activity in a CCK^{BLA}–$D2^{NAcc}$ glutamatergic circuit and establish causality between the CB_1R levels and depression.

Online content

Any methods, additional references, Nature Research reporting summaries, source data, statements of data availability and associated accession codes are available at https://doi.org/10.1038/s41591-018-0299-9.

Received: 31 January 2018; Accepted: 9 November 2018;
Published online: 14 January 2019

References

1. Pezawas, L. et al. 5-HTTLPR polymorphism impacts human cingulate-amygdala interactions: a genetic susceptibility mechanism for depression. *Nat. Neurosci.* **8**, 828–834 (2005).
2. Ashtari, M. et al. Hippocampal/amygdala volumes in geriatric depression. *Psychol. Med.* **29**, 629–638 (1999).
3. Ressler, K. J. & Mayberg, H. S. Targeting abnormal neural circuits in mood and anxiety disorders: from the laboratory to the clinic. *Nat. Neurosci.* **10**, 1116–1124 (2007).
4. Hu, H. Reward and Aversion. *Annu. Rev. Neurosci.* **39**, 297–324 (2016).
5. Russo, S. J. & Nestler, E. J. The brain reward circuitry in mood disorders. *Nat. Rev. Neurosci.* **14**, 609–625 (2013).
6. Proulx, C. D., Hikosaka, O. & Malinow, R. Reward processing by the lateral habenula in normal and depressive behaviors. *Nat. Neurosci.* **17**, 1146–1152 (2014).
7. Hamilton, J. P., Siemer, M. & Gotlib, I. H. Amygdala volume in major depressive disorder: a meta-analysis of magnetic resonance imaging studies. *Mol. Psychiatr.* **13**, 993–1000 (2008).
8. Drevets, W. C., Bogers, W. & Raichle, M. E. Functional anatomical correlates of antidepressant drug treatment assessed using PET measures of regional glucose metabolism. *Eur. Neuropsychopharm.* **12**, 527–544 (2002).
9. Drevets, W. C. et al. A functional anatomical study of unipolar depression. *J. Neurosci.* **12**, 3628–3641 (1992).
10. Hamilton, J. P. & Gotlib, I. H. Neural substrates of increased memory sensitivity for negative stimuli in major depression. *Biol. Psychiatr.* **63**, 1155–1162 (2008).
11. Stuber, G. D. et al. Excitatory transmission from the amygdala to nucleus accumbens facilitates reward seeking. *Nature* **475**, 377–380 (2011).
12. Ambroggi, F., Ishikawa, A., Fields, H. L. & Nicola, S. M. Basolateral amygdala neurons facilitate reward-seeking behavior by exciting nucleus accumbens neurons. *Neuron* **59**, 648–661 (2008).
13. Kim, J., Pignatelli, M., Xu, S. Y., Itohara, S. & Tonegawa, S. Antagonistic negative and positive neurons of the basolateral amygdala. *Nat. Neurosci.* **19**, 1636–1646 (2016).
14. Valverde, O. & Torrens, M. CB1 receptor-deficient mice as a model for depression. *Neuroscience* **204**, 193–206 (2012).
15. Derks, N. M. et al. Cannabinoid modulation of midbrain urocortin 1 neurones during acute and chronic stress. *J. Neuroendocrinol.* **24**, 1447–1461 (2012).
16. Aso, E. et al. BDNF impairment in the hippocampus is related to enhanced despair behavior in CB1 knockout mice. *J. Neurochem.* **105**, 565–572 (2008).
17. Steiner, M. A., Marsicano, G., Wotjak, C. T. & Lutz, B. Conditional cannabinoid receptor type 1 mutants reveal neuron subpopulation-specific effects on behavioral and neuroendocrine stress responses. *Psychoneuroendocrinology* **33**, 1165–1170 (2008).
18. Martin, M., Ledent, C., Parmentier, M., Maldonado, R. & Valverde, O. Involvement of CB1 cannabinoid receptors in emotional behaviour. *Psychopharmacology (Berl.)* **159**, 379–387 (2002).
19. Sanchis-Segura, C., Cline, B. H., Marsicano, G., Lutz, B. & Spanagel, R. Reduced sensitivity to reward in CB1 knockout mice. *Psychopharmacology (Berl.)* **176**, 223–232 (2004).
20. Beyer, C. E. et al. Depression-like phenotype following chronic CB1 receptor antagonism. *Neurobiol. Dis.* **39**, 148–155 (2010).
21. Christensen, R., Kristensen, P. K., Bartels, E. M., Blidda, H. & Astrup, A. Efficacy and safety of the weight-loss drug rimonabant: a meta-analysis of randomised trials. *Lancet* **370**, 1706–1713 (2007).
22. Jiang, W. et al. Cannabinoids promote embryonic and adult hippocampus neurogenesis and produce anxiolytic- and antidepressant-like effects. *J. Clin. Invest.* **115**, 3104–3116 (2005).
23. Bambico, F. R., Katz, N., Debonnel, G. & Gobbi, G. Cannabinoids elicit antidepressant-like behavior and activate serotonergic neurons through the medial prefrontal cortex. *J. Neurosci.* **27**, 11700–11711 (2007).
24. Sherrin, T. et al. Chronic stimulation of corticotropin-releasing factor receptor 1 enhances the anxiogenic response of the cholecystokinin system. *Mol. Psychiatr.* **14**, 291–307 (2009).
25. Bowers, M. E. & Ressler, K. J. Interaction between the cholecystokinin and endogenous cannabinoidsystems in cued fear expression and extinction retention. *Neuropsychopharmacology* **40**, 688–700 (2015).
26. de la Mora, M. P. et al. Role of the amygdaloid cholecystokinin (CCK)/gastrin-2 receptors and terminal networks in the modulation of anxiety in the rat. Effects of CCK-4 and CCK-8S on anxiety-like behaviour and [H-3]GABA release. *Eur. J. Neurosci.* **26**, 3614–3630 (2007).
27. Savanthrapadian, S. et al. Synaptic properties of SOM- and CCK-expressing cells in dentate gyrus interneuron networks. *J. Neurosci.* **34**, 8197–8209 (2014).
28. Medrihan, L. et al. Initiation of behavioral response to antidepressants by cholecystokinin neurons of the dentate gyrus. *Neuron* **95**, 564–576 (2017).
29. Cai, H. J., Haubensak, W., Anthony, T. E. & Anderson, D. J. Central amygdala PKC-delta$^+$ neurons mediate the influence of multiple anorexigenic signals. *Nat. Neurosci.* **17**, 1240–1248 (2014).
30. Wall, N. R., De La Parra, M., Callaway, E. M. & Kreitzer, A. C. Differential innervation of direct- and indirect-pathway striatal projection neurons. *Neuron* **79**, 347–360 (2013).
31. Kreitzer, A. C. & Malenka, R. C. Endocannabinoid-mediated rescue of striatal LTD and motor deficits in Parkinson's disease models. *Nature* **445**, 643–647 (2007).
32. Nestler, E. J. & Carlezon, W. A. The mesolimbic dopamine reward circuit in depression. *Biol. Psychiatr.* **59**, 1151–1159 (2006).
33. Francis, T. C. & Lobo, M. K. Emerging role for nucleus accumbens medium spiny neuron subtypes in depression. *Biol. Psychiatr.* **81**, 645–653 (2017).
34. Golden, S. A., Covington, H. E., Berton, O. & Russo, S. J. A standardized protocol for repeated social defeat stress in mice. *Nat. Protoc.* **6**, 1183–1191 (2011).
35. Francis, T. C. et al. Nucleus accumbens medium spiny neuron subtypes mediate depression-related outcomes to social defeat stress. *Biol. Psychiatr.* **77**, 212–222 (2015).
36. Friedman, A. K. et al. Enhancing depression mechanisms in midbrain dopamine neurons achieves homeostatic resilience. *Science* **344**, 313–319 (2014).
37. Beyeler, A. et al. Divergent routing of positive and negative information from the amygdala during memory retrieval. *Neuron* **90**, 348–361 (2016).
38. Lu, H. C. & Mackie, K. An introduction to the endogenous cannabinoid system. *Biol. Psychiatr.* **79**, 516–525 (2016).
39. Araque, A., Castillo, P. E., Manzoni, O. J. & Tonini, R. Synaptic functions of endocannabinoid signaling in health and disease. *Neuropharmacology* **124**, 13–24 (2017).
40. Piomelli, D. The molecular logic of endocannabinoid signalling. *Nat. Rev. Neurosci.* **4**, 873–884 (2003).
41. Vogel, E., Krabbe, S., Grundemann, J., Cusulin, J. I. W. & Luthi, A. Projection-specific dynamic regulation of inhibition in amygdala micro-circuits. *Neuron* **91**, 644–651 (2016).
42. Eggan, S. M., Melchitzky, D. S., Sesack, S. R., Fish, K. N. & Lewis, D. A. Relationship of cannabinoid Cb1 receptor and cholecystokinin immunoreactivity in monkey dorsolateral prefrontal cortex. *Neuroscience* **169**, 1651–1661 (2010).
43. Shin, S. et al. mGluR5 in the nucleus accumbens is critical for promoting resilience to chronic stress. *Nat. Neurosci.* **18**, 1017–1024 (2015).
44. D'Agostino, G. et al. Appetite controlled by a cholecystokinin nucleus of the solitary tract to hypothalamus neurocircuit. *eLife* **5**, e1225 (2016).
45. Wu, Y. E., Pan, L., Zuo, Y., Li, X. & Hong, W. Detecting activated cell populations using single-cell RNA-seq. *Neuron* **96**, 313–329 e316 (2017).
46. Hamilton, P. J. et al. Cell-type-specific epigenetic editing at the Fosb gene controls susceptibility to social defeat stress. *Neuropsychopharmacology* **43**, 272–284 (2018).
47. Kim, J., Zhang, X. Y., Muralidhar, S., LeBlanc, S. A. & Tonegawa, S. Basolateral to central amygdala neural circuits for appetitive behaviors. *Neuron* **93**, 1464–1479 .e5 (2017).
48. Hoffman, A. F. & Lupica, C. R. Direct actions of cannabinoids on synaptic transmission in the nucleus accumbens: a comparison with opioids. *J. Neurophysiol.* **85**, 72–83 (2001).
49. Grueter, B. A., Brasnjo, G. & Malenka, R. C. Postsynaptic TRPV1 triggers cell type-specific long-term depression in the nucleus accumbens. *Nat. Neurosci.* **13**, 1519–1525 (2010).
50. Lutz, B. Endocannabinoid signals in the control of emotion. *Curr. Opin. Pharmacol.* **9**, 46–52 (2009).
51. Lutz, B., Marsicano, G., Maldonado, R. & Hillard, C. J. The endocannabinoid system in guarding against fear, anxiety and stress. *Nat. Rev. Neurosci.* **16**, 705–718 (2015).
52. Haring, M., Guggenhuber, S. & Lutz, B. Neuronal populations mediating the effects of endocannabinoids on stress and emotionality. *Neuroscience* **204**, 145–158 (2012).
53. Chaudhury, D. et al. Rapid regulation of depression-related behaviours by control of midbrain dopamine neurons. *Nature* **493**, 532–536 (2013).
54. Mathur, B. N. & Lovinger, D. M. Endocannabinoid-dopamine interactions in striatal synaptic plasticity. *Front. Pharmacol.* **3**, 66 (2012).
55. Kreitzer, A. C. & Malenka, R. C. Striatal plasticity and basal ganglia circuit function. *Neuron* **60**, 543–554 (2008).

Acknowledgements

We thank Z. J. Huang (Cold Spring Harbor Laboratory, USA) and M. He (Fudan University, China) for providing CCK-ires-Cre mice; X. Zhang (Qingdao University, China) and F. Wang (The Fourth Military Medical University, China) for providing CB_1R agonist HU210; and Y.-H. Cui (Zhejiang University, China) for stimulating discussions and critical comments. This work was supported by Major Research Plan of the National Natural Science Foundation of China (grant 91432306), Key Project of the National Natural Science Foundation of China (grant 31430034), National Key Research and Development Plan (grant 2016YFA0501000), Non-Profit Central Research Institute Fund

of the Chinese Academy of Medical Sciences (grants 2017PT31038 and 2018PT31041), Funds for Creative Research Groups of China (grant 81521062), Program for Changjiang Scholars and Innovative Research Teams in University and Program of Introducing Talents of Discipline to Universities (grant B13026) to X.-M.L.

Author contributions

C.-J.S. and X.-M.L. designed the research and wrote the manuscript. C.-J.S. performed the in vitro patch–clamp experiments, optogenetic/pharmacogenetic behavioral experiments and immunohistochemical experiments with the help of J.-M.Y., Y.Z., P.S., X.-D.Y., J.-Y.F. and Y.Z. D.Z. performed the virus injections, in vivo recordings and behavioral pharmacological experiments with the help of Q.-X.S., M.-Y.T. and H.-Q.P. K.-X.L. performed the biochemical and in situ hybridization experiments with the help of Y.X. H.H. and S.D. reviewed and edited the manuscript. X.-M.L. supervised all phases of the project.

Competing interests

The authors declare no competing interests.

Additional information

Extended data is available for this paper at https://doi.org/10.1038/s41591-018-0299-9.

Supplementary information is available for this paper at https://doi.org/10.1038/s41591-018-0299-9.

Reprints and permissions information is available at www.nature.com/reprints.

Correspondence and requests for materials should be addressed to X.-M.L.

Publisher's note: Springer Nature remains neutral with regard to jurisdictional claims in published maps and institutional affiliations.

© The Author(s), under exclusive licence to Springer Nature America, Inc. 2019

Methods

Animals. All experiments were reviewed and approved by the Animal Advisory Committee at Zhejiang University and the US National Institutes of Health Guidelines for the Care and Use of Laboratory Animals. Only C57BL/6 J male mice (8–13 weeks old) of normal appearance and weight were used for all behavioral tests, immunohistochemistry, western blot and electrophysiology studies. All mouse lines had been crossed with the C57BL/6 J background for more than ten generations. C57BL/6 J male mice were socially housed, two per cage, and maintained under standard housing conditions on corn cob litter in a temperature (23 ± 1 °C)- and humidity (40%)-controlled animal room on a 12 h light/dark cycle (lights were on from 7:00 to 19:00 every day) with food and water ad libitum until surgery. Following surgery, mice were singly housed. All behavioral tests were conducted during the period of light.

Viruses. The viruses AAV2/9-CaMKIIα-Cre-on-ChR2(H134R)-mCherry (viral: 4.5×10^{12} particles ml^{-1}), AAV2/9-CaMKIIα-Cre-on-Arch3.0-eYFP (viral: 3.6×10^{12} particles ml^{-1}), AAV2/9-CaMKIIα-Cre-on-hM3Dq-mCherry (viral: 3.5×10^{12} particles ml^{-1}) and AAV2/9-CaMKIIα-Cre-on-hM4Di-mCherry (viral: 2.2×10^{12} particles ml^{-1}) were purchased from Shanghai Sunbio Medical Biotechnology. The virus AAV2/9-CaMKIIα-Cre-on-oCHIEF-mCherry (viral: 5.72×10^{12} particles ml^{-1}) used in the HFS-CB_1-LTD experiments was purchased from Taitool Bioscience. The viruses AAV2/9-CaMKIIα-Cre-out-ChR2(H134R)-eYFP (viral:1.8×10^{12} particles ml^{-1}) and AAV2/9-CaMKIIα-Cre-out-Arch3.0-eYFP (viral: 3.6×10^{12} particles ml^{-1}) were purchased from Shanghai Sunbio Medical Biotechnology).

For CB_1R knockdown, the following short-hairpin sequence was used: 5′-GCACTGTTAAGATCGCCAAGG-3′. The specificity and efficiency of the shRNAs were validated and the high titers of engineered AAV (AAV8-CaMKIIα-Cre-on-miR30-shCB_1R-eGFP, 1.94×10^{13} particles ml^{-1}) were produced by Shanghai Sunbio Medical Biotechnology. For monosynaptic rabies tracing, AAV-CAG-DIO-TVA-eGFP (AAV2/9, 2.8×10^{13} particles ml^{-1}), AAV-CAG-DIO-RG (AAV2/9, 6.4×10^{12} particles ml^{-1}) and EnvA-pseudotyped, glycoprotein (RG)-deleted and DsRed-expressing rabies viruses (RV-EvnA-DsRed, RV) (4.8×10^{8} particles ml^{-1}) were provided by F. Xu.

Viral injection and optical fiber/cannula implantation. Mice were anesthetized with sodium pentobarbital (50 mg kg^{-1}, i.p. injection) for bilateral stereotaxic injection of viruses into the BLA (AP: −0.96; ML: ±0.85; DV: −4.95; mm relative to bregma; AP, ML and DV denote anteroposterior, mediolateral and dorsoventral distance from the bregma, respectively). The coordinates were measured from the bregma according to the mouse atlas. We injected 200 nl of virus into each location at a rate of 100 nl min^{-1}. The syringe was not removed until 15–20 min after the end of infusion, to allow diffusion of the virus. After each injection, the needle was left in place for an additional 10 min and then slowly withdrawn.

For the monosynaptic rabies-tracing experiments, Drd1-Cre and Drd2-Cre mice were micro-injected in the NAcc (AP: +1.4; ML: ±0.9; DV: −4.4; mm relative to bregma) with a total 100 nl viral cocktail (1:1) of AAV-CAG-DIO-TVA-eGFP and AAV-CAG-DIO-RG to facilitate the initial infection of NAcc starter neurons. Three weeks later, the same location was injected with 100 nl of the modified rabies virus. One week after the final injection, mice were euthanized and brain sections were collected for confocal imaging.

To allow for projection-specific targeting of BLA CCK or non-CCK glutamatergic terminals in the NAcc, mice were implanted bilaterally with chronic implantable optical fibers (length 5 mm, NA0.22; Newdoon) held in a stainless steel ferrule (RWD Life Science) over the NAcc (AP: +1.4; ML: ±0.9; DV: −4.2; mm relative to bregma). The optical fiber was connected to a laser source using an optical fiber sleeve (Newdoon). Mice performed behavioral tests after habituation.

For pharmacological experiments, a bilateral cannula (RWD Life Science) was implanted above the NAc core (AP: +1.4; ML: ±0.9; DV: −4.3; mm relative to bregma) or medial NAc shell (AP: +1.4; ML: ±0.5; DV: −4.9; mm relative to bregma) for infusion of CB_1R antagonist AM251 (1 μg in 100 nl, Tocris Bioscience) or CB_1R agonist WIN55,212-2 (0.5 μg in 100 nl, Tocris Bioscience). Two stainless steel screws were implanted in the skull for support. The cannula and screws were held in place with dental cement. A stainless steel obturator was inserted into each guide cannula to prevent blockage. Only mice with the correct locations of optical fibers/cannulae and viral expression were used for further analysis.

Ex vivo electrophysiology. Mice were deeply anesthetized with isoflurane (1.5–3.0%). Each brain was removed after decapitation and slices (thickness, 300 mm) were then cut in a solution containing (in mM): 250 sucrose, 26 $NaHCO_3$ 10D (+) glucose, 4 $MgCl_2$, 2.5 KCl, 2.0 sodium pyruvate, 1.25 H_2NaPO_4, 0.5 ascorbic acid, 0.1 $CaCl_2$ and 1.0 kynurenic acid (pH 7.4). Recordings were made at 34 °C (TC-324B; Warner) in artificial cerebrospinal fluid solution containing (in mM): 126 NaCl, 26 $NaHCO_3$, 1.25 NaH_2PO_4, 3.0 KCl, 2.0 $CaCl_2$, 2.0 $MgCl_2$ and 10.0 D-glucose. All external solutions were saturated with 95% O_2/2.5% CO_2 gas.

To evoke synaptic transmission using ChR2, postsynaptic recordings from two neighboring $D2^+$ or $D2^-$ MSNs were made in areas of high ChR2 terminal infectivity in NAcc while activating ChR2 with 473 nm blue light delivered by an LED (Polygon400, Mightex) directed through the objective with a light intensity of <20 mW. Fluorescent cells were visualized under a Nikon Eclipse FN1 microscope (Nikon) equipped with a ×40 water-immersion lens and illuminated with a mercury lamp. We recorded oEPSCs with picrotoxin (100 μM, Tocris Bioscience) added to the cerebrospinal fluid. We recorded mini-EPSCs in the presence of tetrodotoxin (1 μM, MedChemExpress) and picrotoxin (100 μM). All action potential properties and excitability recordings were performed in the presence of 10 μM NBQX (MedChemExpress) and 100 μM picrotoxin.

Biocytin (0.2%, Sigma) was added to the internal solution for neuronal morphology reconstruction. After recording, the micropipette was gently retracted from the cell to achieve an outside-out patch for better morphological reconstruction of biocytin-filled neurons. Slices were fixed with 4% paraformaldehyde in PBS for immunohistochemical staining after recording.

In vivo electrophysiological field potential recording in anaesthetized mice. AAV2/9-CaMKIIα-Cre-on-ChR2-mCherry was injected into BLA of CCK-Cre mice. Fourteen days following injection, mice were anesthetized with isoflurane (4% for induction and 1% for maintenance) and heads were mounted on a stereotaxic frame. The recording optrode comprised a six-channel electrode made of teflon-coated nichrome wire with a central optical fiber. The tip of the fiber extended 0.5 mm beyond the tip of the electrodes. The optrode was lowered, targeting NAcc (AP: +1.4; ML: ±0.9; DV: −4.4; mm relative to bregma). Two stainless steel screws were implanted in the skull for support. The optrodes and screws were held in place with dental cement. For light-evoked stimulation, the optrode was connected to a 473 nm laser. Light pulses at 0.05 Hz were delivered for 2 ms to evoke field EPSP. Once the baseline was stable, baseline oEPSP was recorded for at least 20 min, followed by administration of HU210 (Sigma; 0.05 mg kg^{-1}, i.p.) before continuous recording of oEPSPs for 120 min. The slope of normalized oEPSP was calculated as described (Extended Data Fig. 9a–c)[56–58]. Data were analyzed with a custom-written MATLAB code. The mice were screened as either susceptible or resilient by 10-day CSDS after optrode implantation (Fig. 5p,q). The mice were first injected with virus (AAV-miR30-shCB_1R-eGFP and AAV-CaMKIIα-Cre-on-ChR2-mCherry, 1:1 dilution, total volume 200 nl per side) and then the NAcc was implanted with the optrode (Fig. 6f).

Single-cell RT–PCR. Single-cell RT–PCR was performed as previously described, with certain modifications[59,60]. Cytoplasm was obtained from 10 min whole-cell recordings with an additional 1 min negative pressure under visual control. mRNA was reverse-transcribed to complementary DNA (cDNA) using a QuantiTect Reverse Transcription kit (Qiagen). The entire cDNA was then amplified by multiplex PCR for 25 cycles (94 °C for 40 s, 57 °C for 90 s, 72 °C for 60 s, and a final extension at 72 °C for 10 min) using a Qiagen multiplex PCR master mix kit (Qiagen) in a total volume of 100 μl. A second round of PCR was performed to detect the transcripts of each gene tested using an individual primer set: in a 10 μl reaction, 1 μl of the multiplex PCR mixture was applied as a template with HotStarTaq polymerase (TianGen) and cycled again (35 cycles at 94 °C for 40 s, 57 °C for 40 s, 72 °C for 60 s, and a final extension at 72 °C for 10 min). The final products were run on a GelRed staining 2% agarose gel for visualization under ultraviolet light. Primers for *CCK*, *CaMKIIα* and *CB_1R* were designed according to NCBI published sequences:

Cck (365 base pairs (bp)): forward 5′-GCGTATGTCTGTGCGTGGTG-3′
reverse 3′-TCAAATGCGGGCAGGAAA-5′
CaMKIIα(245 bp): forward 5′-CAGGACGAAGACACCAAAG-3′
reverse 3′-GGATGTGAGGGTTCAGGAT-5′
Cb_1r (295 bp): forward 5′-AGGAGAACGAGGACAACA-3′
reverse 5′-ACATTGGGACTATCTTTGC-3′
To avoid false-negatives, only PCR detections of *Gapdh* were counted.

Immunohistochemistry. Animals that had undergone behavioral analysis were deeply anesthetized with pentobarbital (100 mg kg^{-1}, i.p.) and perfused transcardially with saline followed by 4% PFA in 0.1 MPBS, pH 7.4. Brains were removed, post-fixed overnight in 4% PFA at 4 °C and transferred to 30% sucrose in 0.1 M PBS, pH 7.4. Coronal sections (50 μm) were cut on a cryostat (Leica CM3050 S) and stored in 0.1 M PBS. The sections were incubated in blocking buffer containing 3% bovine serum albumin and 5% normal goat serum in 0.2% Triton X-100/PBS (PBST) for 1 h at room temperature and then with primary antibodies in blocking buffer overnight at 4 °C. The primary antibodies used were: GAD67 (1:400; Millipore, MAB5406), PV (1:5,000, Swant pv27), SOM (1:200, Millipore MAB354), CaMKIIα (1:1,000; Abcam, ab52476) and c-fos (1:5,000, Millipore PC38). After three washes with PBST, sections were incubated with either Alexa Fluor 488– or Alexa Fluor 543–conjugated secondary antibodies at room temperature for 1 h. After another three washes in PBST, sections were incubated with DAPI (1:1,000, Invitrogen, D1306) for 5 min, washed several times and then mounted on Prolong anti-fade medium (Invitrogen), with immunofluorescence assessed using a laser confocal microscope (A1, Nikon). To the biocytin-injected slices we added Alexa Fluor 633–conjugated streptavidin (1:1,000, Invitrogen, S21375) to the secondary antibody solution.

RNAscope in situ hybridization. Coronal brain sections (20 μm) were prepared as described above. Using an RNAscope multiplex fluorescent reagent kit and appropriately designed probes (ACDbio), we performed fluorescence in situ

hybridization according to the manufacturer's standard protocols. Tissue sections were heated for 1 h at 60 °C with a hydrophobic barrier around the perimeter of each section before further processing. Slides showing poor staining were not analyzed.

Immunoblots. Protein samples were prepared from male mice 8–13 weeks old. The mice were decapitated and the brains rapidly removed to ice. Two knife blades were held together with a 1 mm interstice to ensure tissue slice thickness of 1 mm. After removal of the olfactory bulb, a second 1 mm coronal section was selected to dissect the NAcc. Brain tissues were homogenized in RIPA buffer (20 mmol l^{-1} Tris-HCl pH 7.5, 150 mmol l^{-1} NaCl, 1 mmol l^{-1} EDTA, 1% Triton X-100, 0.5% sodium deoxycholate, 1 mmol l^{-1} PMSF and 10 mg ml^{-1} aproptin). A 50 µg protein aliquot from each sample was separated using SDS-polyacrylamide gel electrophoresis and transferred to a nitrocellulose membrane, which was then blocked with 3% non-fat milk in PBS (pH 7.4) for 1 h. The membranes were then incubated with primary antibodies against Cav2.1 (1:1,000; Abcam, ab181371), SNAP25 (1:1,000, Abcam, ab5666), RIMS3 (1:1,000, Abcam, ab192602), CB_1R (1:1,000, Epitomics 8063-1) and GAPDH (1:5,000, Cell Signaling Technology, 5174) overnight at 4 °C. After washing three times in 0.1% Tween 20 in TBS, the membranes were incubated with horseradish peroxidase–conjugated anti-rabbit secondary antibodies (1:3,000, Abcam, ab136817) in 3% non-fat milk for 1 h at room temperature and then visualized with an ECL kit (Thermo Scientific). Quantitative analysis was performed with ImageJ software. All experiments were performed at least three times. The data for statistical analyses were derived from at least three mice per group.

Behavioral assays. For ChR2-mediated stimulation and Arch-mediated inhibition experiments, the optical fibers were connected to a 473 nm blue laser diode and a 563 nm yellow laser diode, respectively. Laser power was adjusted to 10–15 mW before each experiment. Measurements were made from bilateral fibers, with the assumption that half the power would be delivered to each hemisphere.

Real-time place preference/aversion. On day 1, mice were placed in a Plexiglas box with two interconnecting chambers (length 50 cm × width 50 cm × height 50 cm for each chamber) for 15 min and allowed to freely explore the chambers. One chamber was randomly designated as the stimulation chamber, the other as the no-stimulation chamber. The percentage of time spent in the stimulation chamber was measured at baseline, and mice with a bias for one side were excluded. On day 2, mice were randomly placed in either chambers and received 20 Hz blue light pulses from the time they entered the stimulation chamber until they entered the no-stimulation chamber. The time spent in each chamber was measured for 10 min. The travel traces and time spent in each chamber were recorded by an ANY-maze behavioral recording system. Preference score was calculated as (time in stimulated side – time in non-stimulated side)$_{test}$ – (time in stimulated side – time in non-stimulated side)$_{baseline}$.

Negative and positive reinforcement procedures. Three weeks after virus injection, mice with a cannula placed above the NAc were prepared for nose-poke training. We food-restricted a separate group of mice to 90% of their free-feeding bodyweight. The mice were then trained for one session per day for 1 h in the operant chambers (Anilab Software & Instruments Co., Ltd.) on a FR1 schedule (in which each nose poke resulted in 20 µl of 15% sucrose solution, wt vol^{-1}). In addition, a tone and house-light cue were turned on for 2 s. Once the mice reached stable behavioral responses (as determined by 3 days of >100 active nose pokes that varied by ≤20% from the first of the three days).

For freely moving optical self-stimulation, mice received 2 s of 20 Hz optical stimulation time-locked to the cue following each active nose poke. For optical stimulation during sucrose reinforcement, mice received 2 s of 20 Hz optical stimulation time-locked to the active nose pokes, after which they earned a sucrose reward. Both active and inactive nose-poke time stamp data were recorded using Anilab software and analyzed with Matlab and Microsoft Excel software.

NAcc micro-injection before optical stimulation. Stylets were removed from guide cannulae and a 26-gauge injector needle connected to a 1 ml Hamilton syringe was inserted. All micro-injections were delivered in 100 nl sterile saline at a rate of 100 nl min^{-1}. Injector needles remained in place for an additional 2 min before being removed and replaced immediately with the stylets or optical fibers for self-stimulation sessions.

10-day chronic social defeat stress. Chronic social defeat stress was carried out as described previously[61]. In brief, before the experiment, retired male breeder CD1 mice were screened on three consecutive days to validate their aggressive characteristics. Over the following ten consecutive days, each experimental male C57BL6/JL mouse (intruder) was introduced into the home cage of a novel aggressive CD1 mouse (resident) for 10 min and was then physically defeated. After 10 min of physical interaction, residents and intruders were maintained in sensory contact for 24 h using a perforated Plexiglass partition dividing the resident home cage in two. After 10 days of CSDS, animals were housed singly and tested 24 h later for social avoidance behavior. Control animals were housed in pairs, one on each side of a perforated Plexiglass partition, and they were never in physical or sensory contact with CD1 mice.

Social interaction. Social avoidance behavior was measured according to a two-stage social interaction test. In the first stage, animals were placed in an open-field arena (44 × 44 × 44 cm^3) containing an empty metal cage (9.5 × 9.5 × 8 cm^3). In all behavioral experiments, the animals' tracks were monitored with ANYMAZE video-tracking software. Time spent in the area surrounding the cage (interaction zone, an 8 cm region flanking the cage) and in the area along the wall opposite the cage (opposing zone, 9 cm region along the wall opposite the cage) were measured individually. The time spent in the interaction zone in this first stage was termed 'No target.' Animals were then returned to the home cage for 1 min. In the second stage, a novel, aggressive CD1 mouse was placed in the cage and the same metrics were measured (Target). From these two stages, a social interaction index was calculated (time spent in interaction zone in Target/time spent in interaction zone in No target). Animals were deemed susceptible when this index was <1 and resilient when the index was >1.

In a subset of studies, susceptible mice underwent three consecutive days of repeated bilateral light/chemical-genetic stimulation to inhibit the CCK^{BLA}–$D2^{NAcc}$ circuit during a 10 min sensory stress period after 10 days of chronic social defeat stress.

Two-trial subthreshold social defeat stress. A two-trial subthreshold social defeat stress experiment was performed as described previously[53]. The subthreshold paradigm involved placing the test mouse (intruder) into the home cage of a larger, retired resident breeder mouse (CD1) for 10 min, during which time the former was physically attacked (defeated) by the latter. After 10 min of physical interaction, the intruder underwent 10 min of sensory stress. For this, a perforated Plexiglass partition was placed in the middle of the CD1 mouse's home cage, with the two mice physically separated but in proximity to each other. After 10 min of sensory stress, the intruder was returned to its home cage for 5 min after which it went through a second round of physical interaction and sensory stress in the home cage of a new CD1 mouse. After two defeat bouts, the intruder was returned to its home cage and underwent social interaction testing the following day.

In a subset of experiments, the experimental mice underwent either bilateral light/chemogenetic stimulation or intra-NAcc cannular infusion of AM251, to stimulate the CCK^{BLA}–$D2^{NAcc}$ circuit or antagonism to CB_1R during the sensory stress period in SSDS.

Three-day subthreshold social defeat stress. This procedure[43] was identical to the normal chronic social defeat stress procedure, with the exception that the procedure lasted for three consecutive days.

Sucrose preference test. After completion of the social interaction test, mice were habituated to 50 ml tubes with stoppers fitted with ballpoint sipper tubes (a two-bottle choice) filled with drinking water for two consecutive days. After habituation, the mice were given access to a two-bottle choice of water or 1% sucrose solution. Bottles containing water and sucrose were weighed at several time points, 09:00, 15:00 and 18:00, for a further 2 days. The position of the bottles was changed (left to right, right to left) after each weight measurement to ensure that the mice did not develop a side preference. Sucrose preference was calculated as the percentage (amount of sucrose consumed × 100 (bottle A)/total volume consumed (bottles A + B)). Total sucrose consumption over the two days was measured and used to obtain sucrose preference.

Tail-suspension test. Twenty-four hours after completion of the sucrose preference test, the mice underwent the tail-suspension test. Briefly, they were suspended by their tails with adhesive tape (1 cm from the tail tip) and roughly 50 cm above the surface so no contact could be made. Plastic tubes were placed over the tails to ensure they could neither climb nor hang on to their tail. The animals were video recorded for 5 min, and the time spent immobile was quantitated over the full 5 min post hoc.

Open-field test. Mice were individually introduced to the central zone of an open-field (40 × 40 cm^2) chamber with dim light in the dark phase for 10 min. Their paths were recorded by video camera and analyzed with Noldus software. A blue light (473 nm) was intermittently turned on and off for periods of 60 s. Locomotor activity was evaluated as total distance traveled. Anxiety-like behavior was defined by the distance traveled in the central zone.

Elevated plus maze. The elevated plus maze apparatus comprised two open arms (30 × 5 cm^2) and two closed arms (30 × 5 × 20 cm^3) elevated 50 cm above the surface. Mice were placed in the center facing one of the two open arms and allowed to explore for 6 min. Anxiety-like behavior was assessed by time and distance traveled within the open arms.

Quantification and statistical analyses. All experiments and data analyses were conducted blinded, including the immunoblots, immunohistochemistry, electrophysiology and behavioral analyses. The number of replicates (n) is

indicated in the figure legends and refers to the number of experimental subjects independently treated in each experimental condition. Data are presented as means ± s.e.m. Statistical comparisons were performed using SPSS (version 17.0) with appropriate inferential methods, as indicated in the figure legends. Normally distributed data were tested by one- and two-way analysis of variance (ANOVA) followed by post hoc Scheffe's test for multiple comparisons, and unpaired and paired two-sample Student's *t*-test for two-group comparisons. Non-normally distributed data were analyzed by Mann–Whitney *U*-tests. No statistical methods were used to pre-determine sample size, or to randomize. Statistical significance was set at $^{*}P<0.05$, $^{**}P<0.01$, $^{***}P<0.001$, $^{****}P<0.0001$.

Reporting Summary. Further information on experimental design is available in the Nature Research Reporting Summary linked to this paper.

Data availability

The datasets that support the findings of this study are available from the corresponding author upon reasonable request. All requests for raw and analyzed data and materials are promptly reviewed by the Center of Neuroscience of Zhejiang University to verify whether the request is subject to any intellectual property or confidentiality obligations. Any data and materials that can be shared will be released via a Material Transfer Agreement.

References

56. Han, J. et al. Acute cannabinoids impair working memory through astroglial CB1 receptor modulation of hippocampal LTD. *Cell* **148**, 1039–1050 (2012).
57. Zhou, T. et al. History of winning remodels thalamo-PFC circuit to reinforce social dominance. *Science* **357**, 162–168 (2017).
58. Xiong, Q., Znamenskiy, P. & Zador, A. M. Selective corticostriatal plasticity during acquisition of an auditory discrimination task. *Nature* **521**, 348–351 (2015).
59. Toledo-Rodriguez, M. & Markram, H. Single-cell RT–PCR, a technique to decipher the electrical, anatomical, and genetic determinants of neuronal diversity. *Meth. Mol. Biol.* **403**, 123–139 (2007).
60. Li, Y. et al. A distinct entorhinal cortex to hippocampal CA1 direct circuit for olfactory associative learning. *Nat. Neurosci.* **20**, 559–570 (2017).
61. Berton, O. et al. Essential role of BDNF in the mesolimbic dopamine pathway in social defeat stress. *Science* **311**, 864–868 (2006).

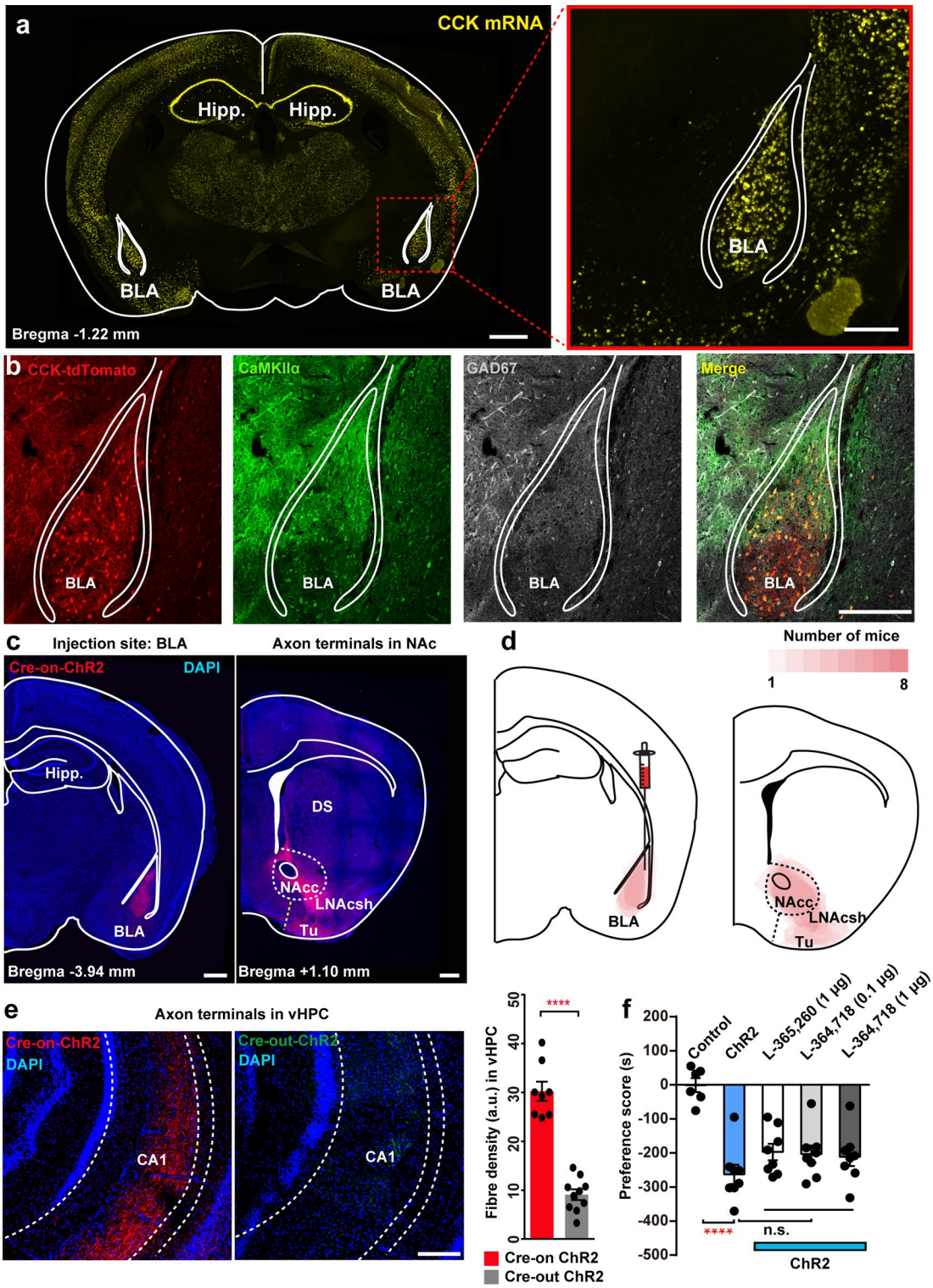

Extended Data Fig. 1 | *CCK* mRNA expression in BLA and the downstream targets of BLA CCK glutamatergic neurons. a, Left, coronal representative brain image of *CCK* mRNA in BLA; scale bar, 500 μm. Right, magnified view of BLA; scale bar, 200 μm. **b**, Zoomed-out view of BLA CCK-tdTomato neurons (red) from a CCK-ires-Cre::Ai14 mouse co-immunostained for CaMKIIα and GAD67. Scale bar, 200 μm. **c**, Coronal brain slice (stained with DAPI) from a CCK-ires-Cre mouse with AAV-CaMKIIα-Cre-on-ChR2-mCherry (**a**) virus injected into BLA (left, injection site) and its axonal terminals in NAcc (right); scale bars, 200 μm for BLA and 300 μm for NAcc. **d**, Overlay of Cre-on-ChR2-mCherry ($n = 8$ mice) expression areas in BLA (left, injection site) or NAcc (right). **e**, Representative image (left) and quantification (right) of axonal terminals in vHPC of Cre-on-ChR2-mCherry or Cre-out-ChR2-eYFP virus-injected mice; scale bar, 200 μm. Two-sided unpaired *t*-test, $t = 9.942$, d.f. = 16, $P < 0.0001$, $n = 8$, 10 mice for each group, respectively. **f**, Quantification of in vivo optogenetic activation of $CCK^{BLA\text{-}NAcc}$ glutamatergic neurons, with intra-NAcc local infusion of L-365,260 (CCK_A receptor antagonist, 1 μg in 200 nl) or L-364,718 (CCK_B receptor antagonist, 0.1 μg or 1 μg in 200 nl) in NAcc during real-time place avoidance. One-way ANOVA, $F_{(4, 33)} = 12.97$, $P < 0.0001$, $n = 6, 8, 8, 8, 8$ mice for each group. All data are means ± s.e.m. ****$P < 0.0001$; n.s., no significance.

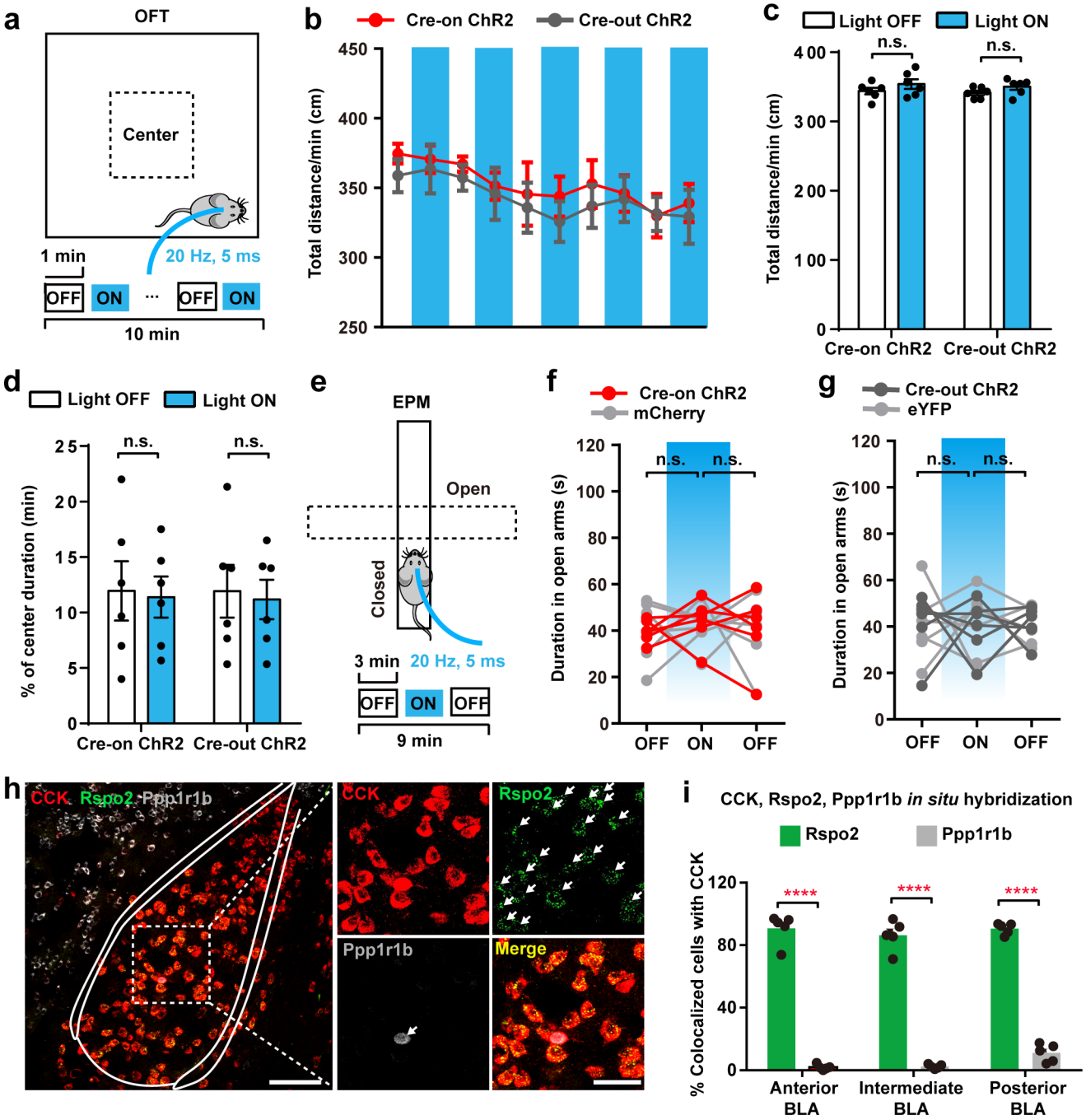

Extended Data Fig. 2 | *CCK, Rspo2, Ppp1r1b* mRNA expression in BLA and optogenetic manipulation changes neither locomotion nor anxiety. a, Schematic of open-field test (OFT) with intermittent photostimulation. **b**, Mean total distance per minute across 10 min OFT in Cre-on ChR2 or Cre-out ChR2 mice. **c**,**d**, Quantification of total distance per minute (**c**) and duration in center zone (**d**) in light ON and OFF periods from Cre-on ChR2 or Cre-out ChR2 mice. Two-way ANOVA in **c**, $F_{(1, 10)} = 0.01743$, $P = 0.8976$. Two-way ANOVA in **d**, $F_{(1, 10)} = 0.002206$, $P = 0.9635$, $n = 6$, 6 mice for Cre-on ChR2 and Cre-out ChR2 groups, respectively. **e**, Schematic of elevated plus maze (EPM) with intermittent photostimulation. **f**,**g**, Duration spent within open arms in light ON and OFF periods for mice expressing Cre-on-ChR2 (or mCherry control, **f**) or Cre-out-ChR2 (or eYFP control, **g**) virus in BLA. Two-way ANOVA in **f**, $F_{(2, 20)} = 0.02805$, $P = 0.9724$, $n = 6$, 6 mice for mCherry and Cre-on ChR2 groups, respectively. Two-way ANOVA in **g**, $F_{(2, 20)} = 0.005046$, $P = 0.9950$, $n = 6$, 6 mice for mCherry and Cre-out ChR2 groups, respectively. **h**, Left, representative images *CCK*, *R-spondin 2* (*Rspo2*) and *protein phosphatase 1 regulatory subunit 1B* (*Ppp1r1b*) mRNA expression in BLA, scale bar 100 μm. Right, representative image showing magnified view of white rectangle; arrows indicate neurons co-labeled with CCK mRNA; scale bar, 50 μm. **i**, Quantification of *CCK* mRNA co-labeled with *Rspo2* or *Ppp1r1b* mRNA. Two-way ANOVA, $F_{(2, 24)} = 1.371$, $P = 0.2730$, $n = 926$, 1220, 480 CCK-positive neurons for anterior, intermediate and posterior BLA from 5 mice. All data are means ± s.e.m. ***$P < 0.001$; ****$P < 0.0001$; n.s., no significance.

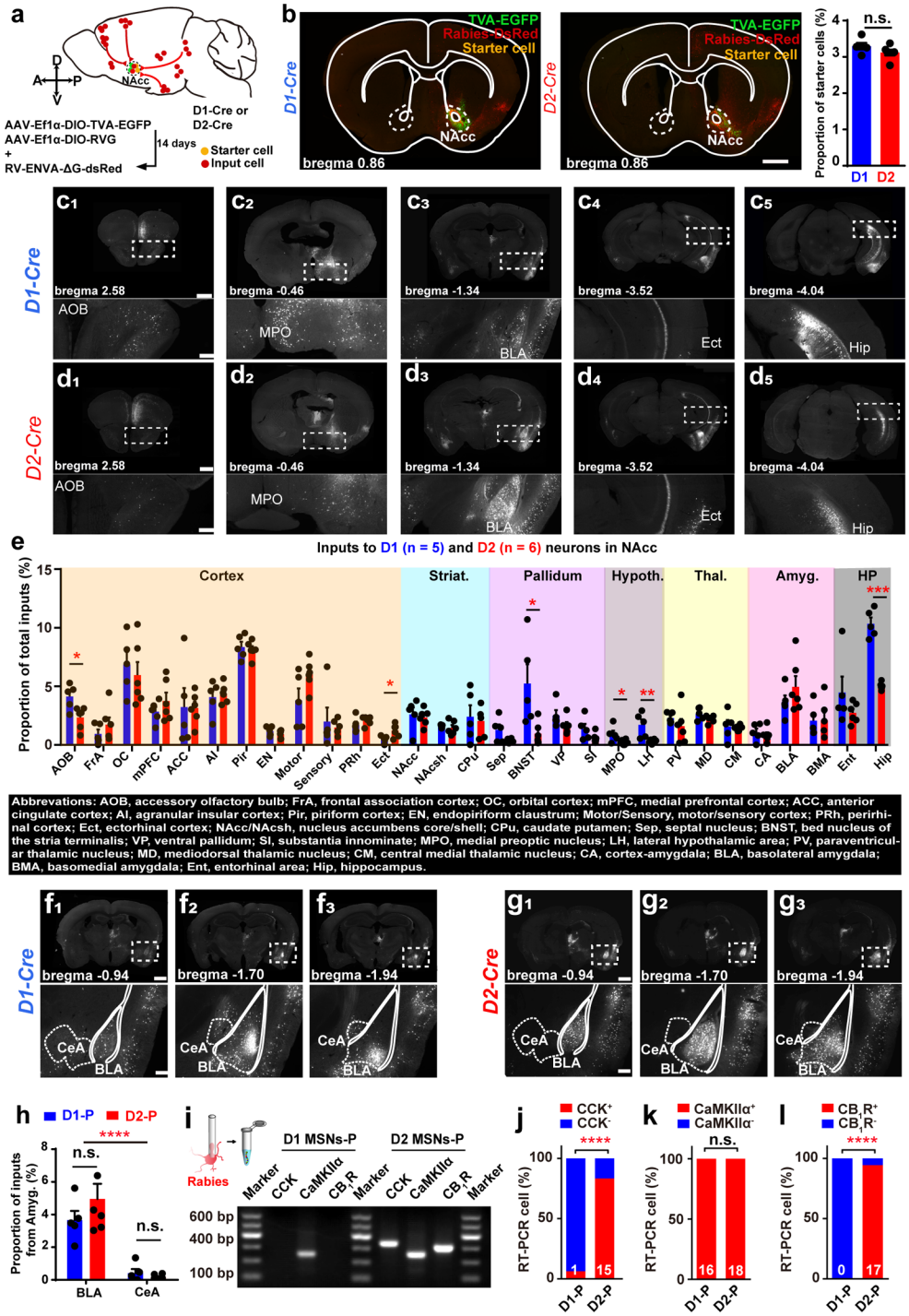

Extended Data Fig. 3 | Quantitative analysis of whole-brain inputs to D1 and D2 MSNs in NAcc. a, Monosynaptic retrograde rabies tracing from D1 and D2 neurons in NAcc. **b**, Left, coronal sections through NAcc of D1-Cre (left) and D2-Cre (right) tracing brains showing location of starter cells; scale bar, 1 mm. Right, quantification of starter cells in D1-Cre ($n = 5$) and D2-Cre ($n = 6$) mice. Two-sided unpaired t-test, $t = 1.4443$, d.f. $= 9$, $n = 5$, 6 mice for each group. **c**,**d**, Top, coronal sections of a D1-Cre (**c**) and a D2-Cre (**d**) tracing brain showing distribution of presynaptic partners; scale bar, 1 mm. Bottom, magnified images of rectangular regions in top images; scale bar, 250 μm. **e**, Inputs to D1 ($n = 5$) and D2 ($n = 6$) neurons from whole-brain regions, shown as proportion of total number of cells counted that are located in a region. Striat, striatum;hypoth, hypothalamus; thal, thalamus; amyg, amygdala; HP, hippocampus. Two-way ANOVA, $F_{(28,261)} = 3.141$, $P < 0.0001$, $n = 5$, 6 mice for each group. **f**,**g**, Top, coronal sections of D1-Cre (**f**) and D2-Cre (**g**) tracing brains showing distribution of presynaptic partners in anterior (**f1**,**g1**), intermediate (**f2**,**g2**) and posterior (**f3**,**g3**) parts of amygdala; scale bar, 1 mm. Bottom, magnified images of rectangular regions in top images; scale bar, 200 μm. **h**, Comparison between NAcc D1-projecting (D1-P) and D2-projecting (D2-P) neurons in BLA and CeA. Two-way ANOVA, $F_{(1,18)} = 1.753$, $P = 0.2021$, $n = 5$, 6 mice for each group. **i**, Detection of CCK, CaMKIIα and CB_1 transcripts in rabies-labeled BLA neurons by single-cell RT-PCR. **j–l**, Percentages of cells positive for CCK (**j**), CaMKIIα (**k**) and CB_1 (**l**) in D1-P ($n = 16$ neurons from 5 mice) or D2-P ($n = 18$ neurons from 5 mice) neurons in BLA (rabies-DsRed identified). Fisher's exact test, $P < 0.0001$ in **j**, $P = 1.0$ in **k**, $P < 0.0001$ in **l**. All data are means ± s.e.m. $^*P < 0.05$; $^{**}P < 0.01$; $^{***}P < 0.001$; $^{****}P < 0.0001$; n.s., no significance.

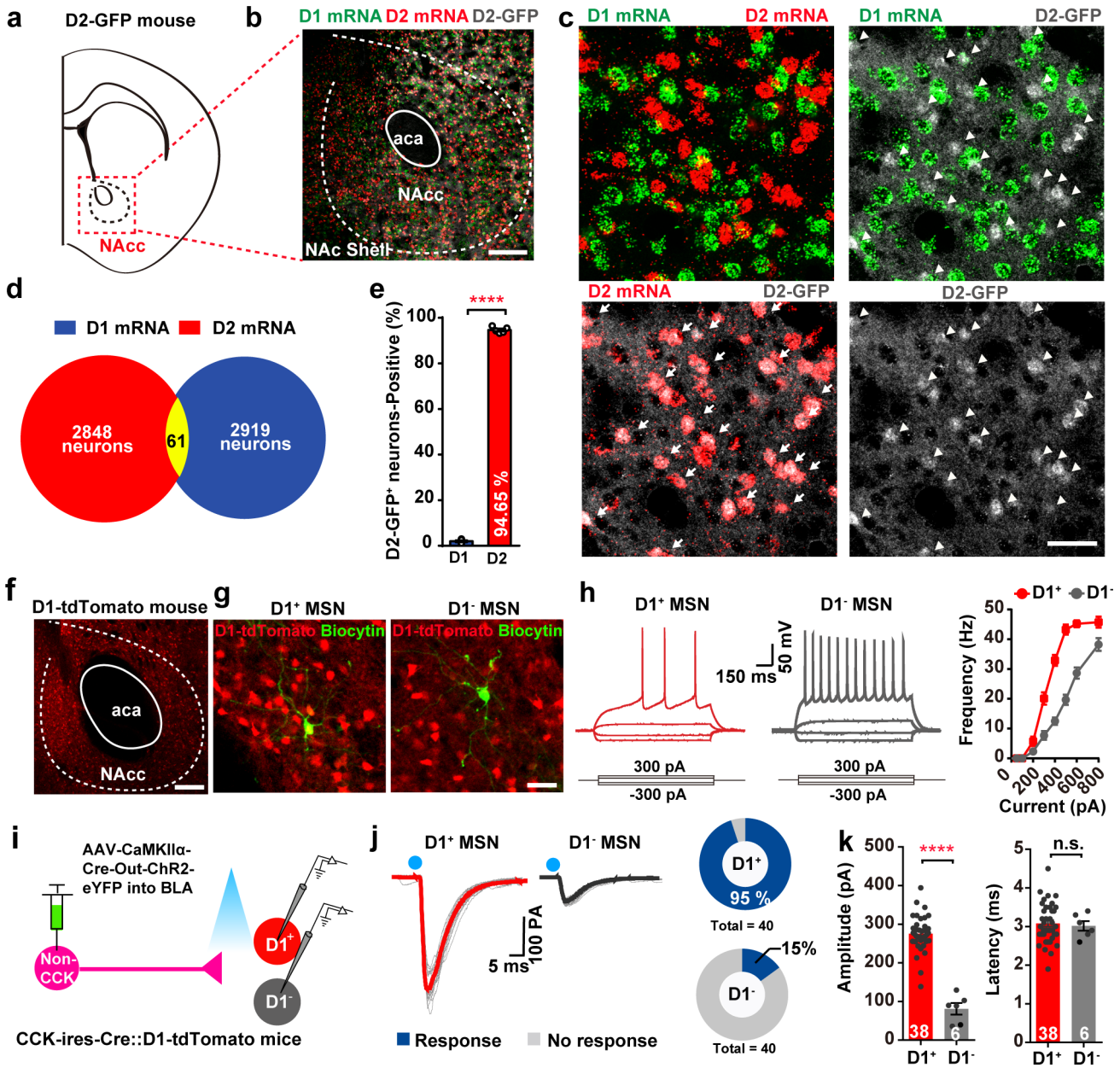

Extended Data Fig. 4 | Evidence of target specificity in D2-GFP and D1-tdTomato mice. a,**b**, Schematic (**a**) and representative images (**b**) of NAcc from a D2-GFP mouse, triple-labeled for D2–GFP, D1 and D2 mRNA, scale bar, 200 µm. **c**, Magnified view from **b**. Arrowheads indicate $D2^{-}GFP$-positive neurons whereas arrows indicate co-labeled neurons with D2–GFP; scale bar, 50 µm. **d**, Scaled Venn diagram showing number of D1- and D2-mRNA-positive neurons in NAcc. **e**, Percentage of NAcc D1–and D2-mRNA-positive neurons co-labeled with D2-GFP-positive neurons ($D2\text{-}GFP^{+}$). Two-sided unpaired *t*-test in **e**, $t = 133.3$, d.f. = 8, $P < 0.0001$, $n = 2658$ $D2\text{-}GFP^{+}$ neurons in total from 5 mice. **f**, Representative image of D1-tdTomato-labeled neurons in NAcc of D1-tdTomato mice; scale bar, 40 µm. **g**, Representative images of recorded D1-tdTomato-positive ($D1^{+}$, left) and D1-tdTomato-negative ($D1^{-}$, right) neurons in NAcc using in vitro slice recording. Biocytin was used to indicate recorded neurons; scale bar, 20 µm. **h**, Representative traces (left) of whole-cell current clamp recordings from $D1^{+}$ ($n = 16$ neurons from 3 mice) or $D2^{-}$($n = 16$ neurons from 3 mice) MSNs in vitro and current and voltage (*I–V*) curves (right) of $D1^{+}$ and $D1^{-}$ MSNs. Raw traces show individual voltage responses to a series of 600 ms current pulses from −300 to 300 pA in 200 pA steps. **i**, Schematic showing tested connections in CCK-ires-Cre::D1-tdTomato mice; non-CCK neurons were transduced by injection of AAV-CaMKIIα-Cre-out-ChR2-eYFP in BLA. **j**, Left, light responses recorded from two adjacent $D1^{+}$ or $D1^{-}$ MSNs following 5 ms laser stimulation of non-CCK terminals from BLA. Right, connectivity charts are shown. **k**, Quantification of amplitude (left) and latency (right) of oEPSCs recorded in NAcc $D1^{+}$ and $D1^{-}$ MSNs from non-CCK glutamatergic neurons. Two-sided unpaired *t*-test, $t = 9.863$, d.f. = 42, $P < 0.0001$, in amplitude. $t = 0.2955$, d.f. = 42, $P = 0.7691$; in latency. $n = 38$ out of 40 $D1^{+}$ MSNs (95%) and 6 out of 40 $D1^{-}$ MSNs (15%) from 6 mice. All data are means ± s.e.m. $^{****}P < 0.0001$; n.s., no significance.

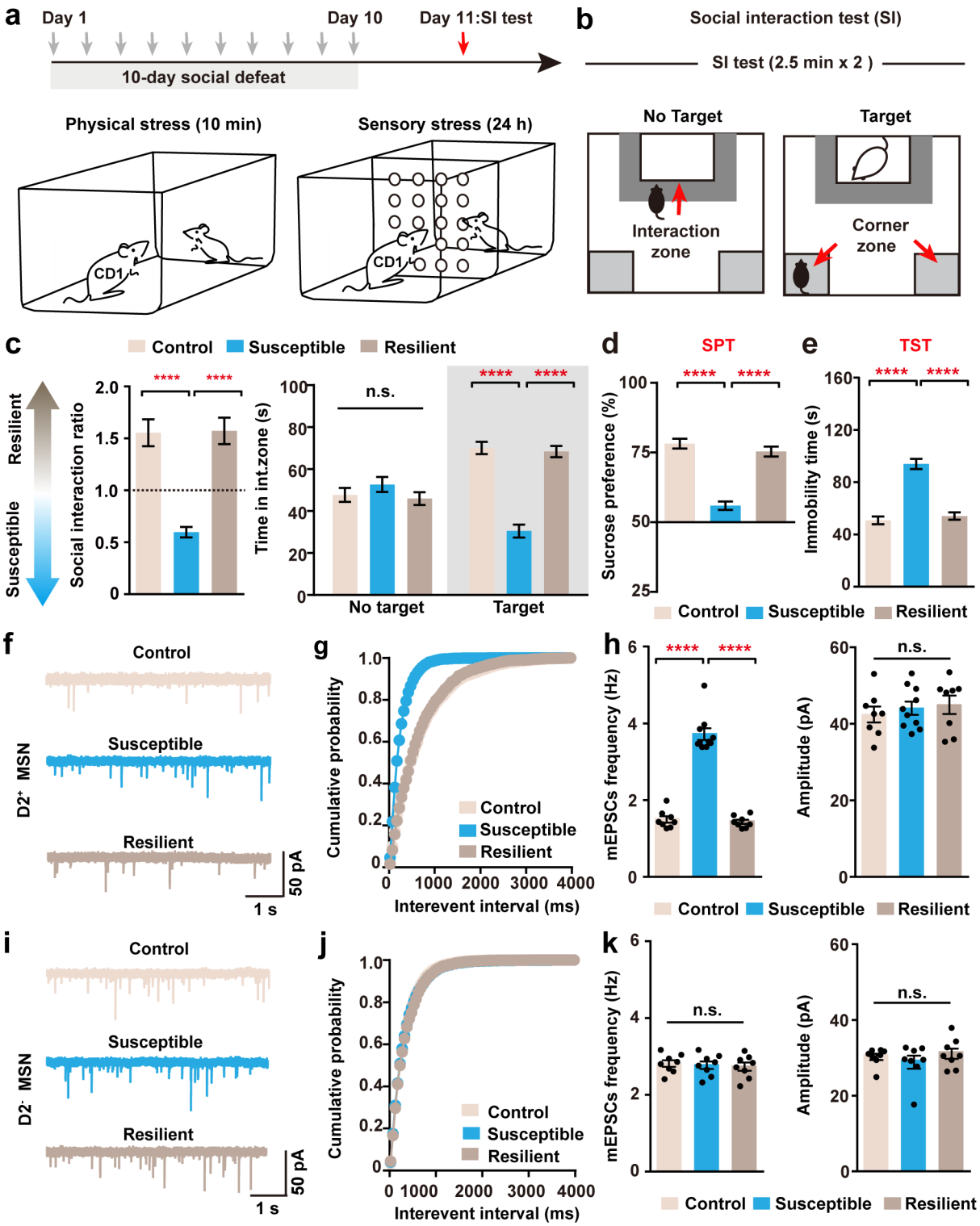

Extended Data Fig. 5 | mEPSC frequencies are increased in D2$^+$ neurons in susceptible mice. a,**b**, Schematic of 10-day chronic social defeat stress (10-d CSDS) procedure (**a**) and social interaction test (SI, **b**). **c**, Left, distribution of interaction ratios. One-way ANOVA, $F_{(2, 39)}=76.55$, $P<0.0001$, $n=12, 16, 14$ mice for each group. Right, quantification in social interaction showing that susceptible mice spent less time interacting with a novel CD1 mouse, whereas resilient mice interacted the same as control mice. Two-way ANOVA, $F_{(2, 39)}=50.58$, $P<0.001$, $n=12, 16, 14$ mice for each group. **d**,**e**, Sucrose preference in sucrose preference test (SPT) was decreased and total immobility time in tail-suspension test (TST) was increased in susceptible mice. One-way ANOVA in **d**, $F_{(2, 39)}=59.02$, $P<0.001$. One-way ANOVA in **e**, $F_{(2, 39)}=52.59$, $P<0.001$, $n=12, 14, 16$ mice for each group. **f**,**i**, Example mEPSC traces, measured in a whole-cell configuration of D2$^+$ (**f**) or D2$^-$ neurons (**i**) in NAc. **g**,**j**, Cumulative distribution of mEPSC inter-event intervals of D2$^+$ (**g**) and D2$^-$ (**j**) MSNs recorded in NAcc. **h**,**k**, Average mEPSC frequency (left) and amplitude (right) measured in D2$^+$ (**h**) and D2$^-$ (**k**) MSNs. One-way ANOVA of frequency (**h**, D2$^+$), $F_{(2, 23)}=135.0$, $P<0.0001$. One-way ANOVA in amplitude (**h**, D2$^+$), $F_{(2, 23)}=0.3686$, $P=0.6957$, $n=8, 10, 8$ neurons, each from 4 mice. One-way ANOVA of frequency (**k**, D2$^-$), $F_{(2, 21)}=0.1732$, $P=0.8422$. One-way ANOVA in amplitude (**k**, D2$^-$), $F_{(2, 21)}=0.6912$, $P=0.5120$, $n=8, 8, 8$ neurons, each from 4 mice, respectively. All data are means ± s.e.m.$^{****}P<0.0001$; n.s., no significance.

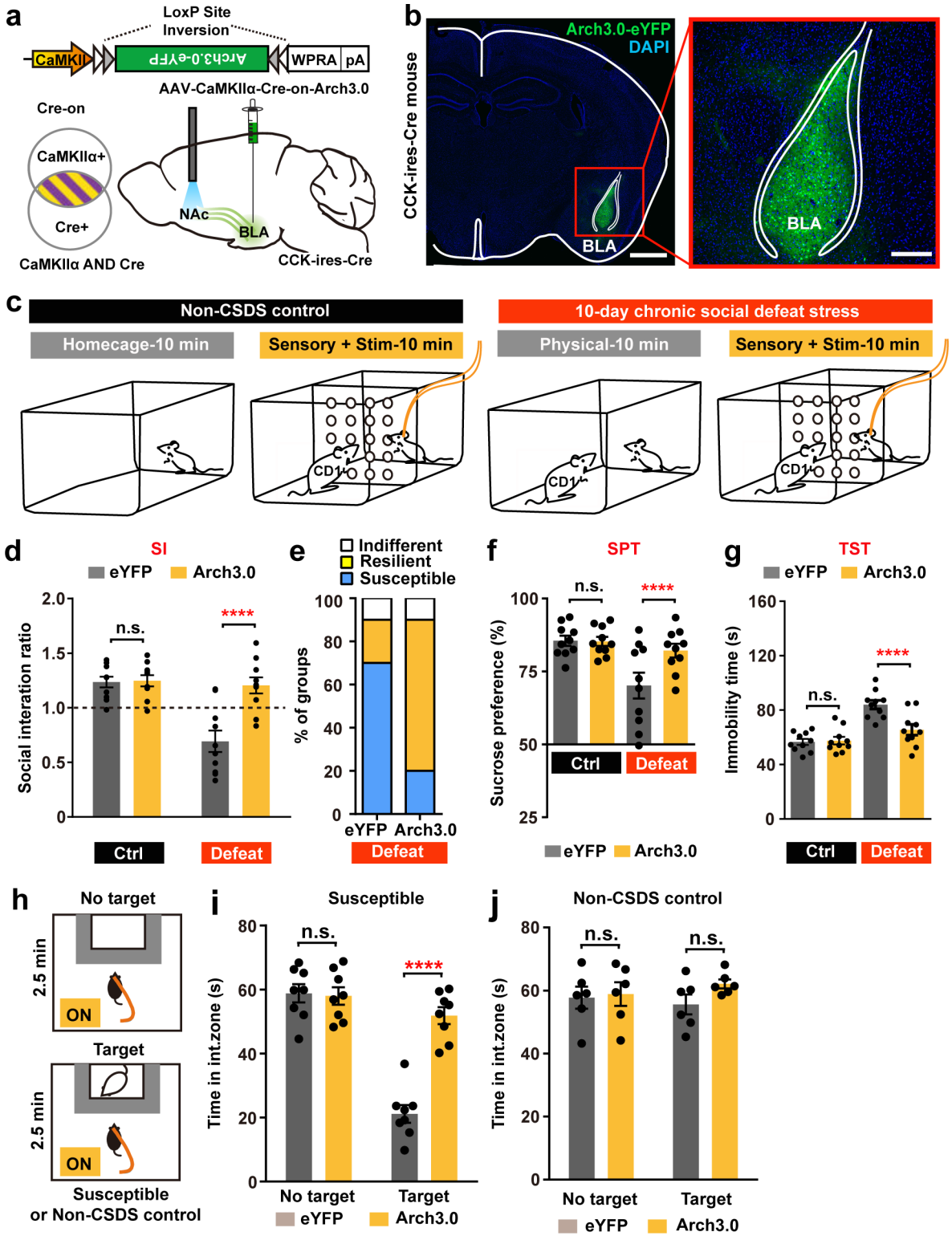

Extended Data Fig. 6 | Photo-inhibition of CCK^{BLA}–D2^{NAcc} circuit prevents the acquisition and expression of social avoidance. a, Schematic of virus injection to express Arch3.0 in BLA CCK neurons and optical fiber implantation in NAcc. **b**, Left, Arch3.0-eYFP expression in BLA; scale bar, 1 mm. Right, magnified image; scale bar, 200 μm. **c**, Daily photo-inhibition of CCK^{BLA}–D2^{NAcc} circuit during 10 min of sensory contact in non-CSDS control mice (left) and susceptible mice (right, after 5 min physical aggression). **d**, Social interaction ratio in each group. Two-way ANOVA, $F_{(1,36)}=12.53$, $P=0.0011$, $n=10$, 10, 10, 10 mice for each group. **e**, Proportions of susceptible, indifferent and resilient mice in eYFP and Arch3.0 group (defeat). **f**, Sucrose preference in SPT. One-way ANOVA, $F_{(3,36)}=16.72$, $P<0.0001$, $n=10$, 10, 10, 10 mice for each group. **g**, Total immobility time in TST. One-way ANOVA, $F_{(3,36)}=6.847$, $P=0.0009$, $n=10$, 10, 10, 10 mice for each group. **h**, Schematic of phasic photo-inhibition of the CCK^{BLA}–D2^{NAcc} circuit during 2.5 min social interaction test. **i**,**j**, Quantification of time in social interaction zone in susceptible mice (**i**) and non-CSDS control mice (**j**) expressing either eYFP or Arch 3.0. Two-way ANOVA in **i**, $F_{(1,28)}=32.66$, $P<0.0001$. Two-way ANOVA in **j**, $F_{(1,20)}=0.7574$, $P<0.0001$, $n=8$, 8 mice for each group, respectively. Two-way ANOVA in **j**, $F(1,20)=0.7574$, $P=0.3945$, $n=6$, 6 mice for each group, respectively. All data are means ± s.e.m. ****$P<0.0001$; n.s., no significance.

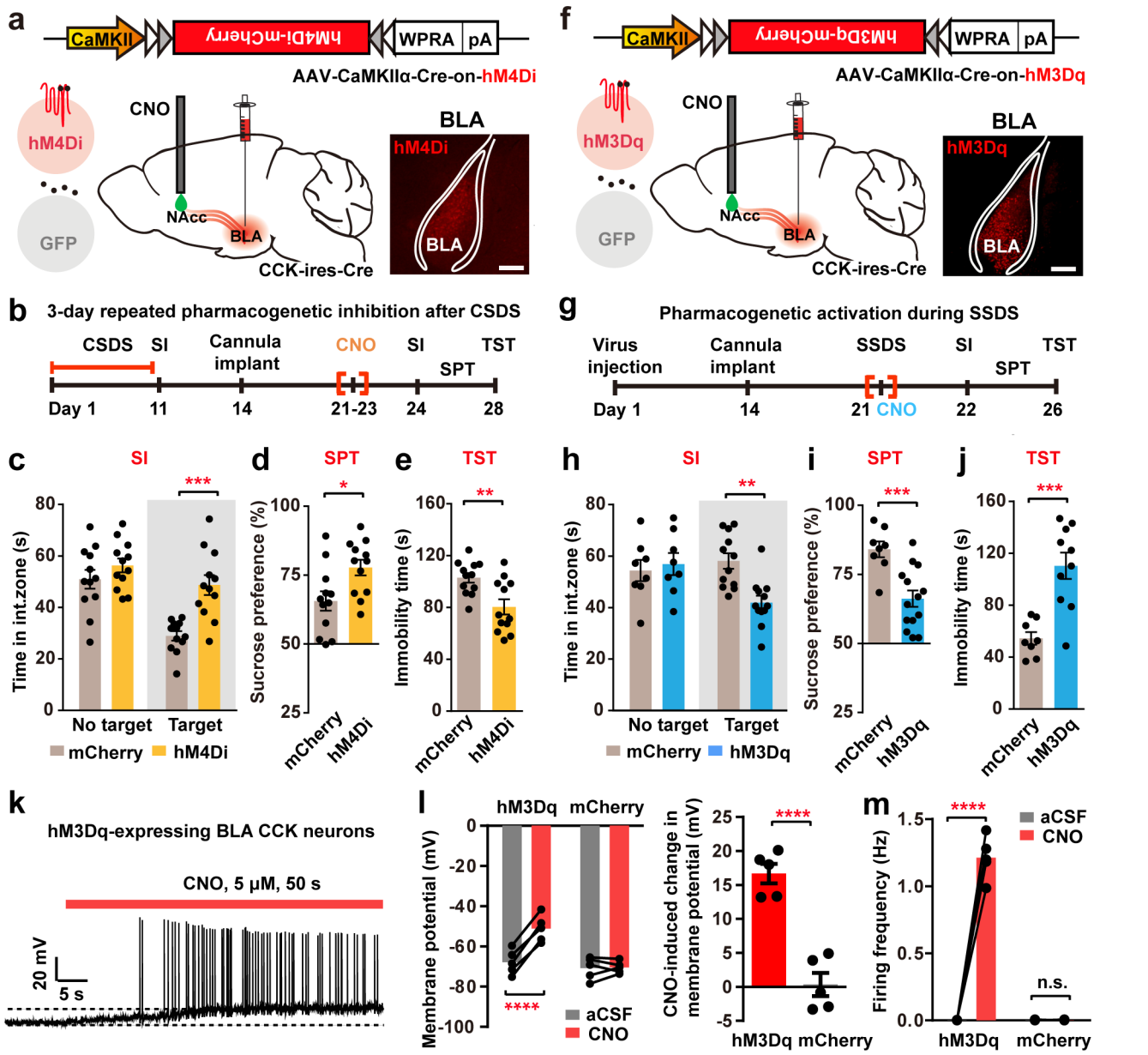

Extended Data Fig. 7 | Pharmacogenetic bidirectional effects of modulating CCK^{BLA}–D2^{NAcc} circuit on stress susceptibility. a,**f**, Schematic illustrating AAV-CaMKIIα-Cre-on-hM4Di-mCherry (**a**) and AAV-CaMKIIα-Cre-on-hM3Dq-mCherry (**f**) viralbilateral injection into BLA of CCK-ires-Cre mice and cannula implantation in NAcc for local infusion of CNO (3 μM, 100 nl). Intra-NAcc infusion of CNO via cannula selectively inhibits/activates synaptic activity via hM3Dq- or hM4Di-mediated activation or inhibition in NAcc, respectively. **b**,**g**, Paradigms of 3-day repeated pharmacogenetic inhibition of the CCK^{BLA}–D2^{NAcc} circuit in susceptible mice following 10 days of chronic social defeat stress (CSDS) (**b**), or acute pharmacogenetic activation of CCK^{BLA}–D2^{NAcc} circuit during social interaction in a two-trial subthreshold social defeat stress (SSDS) paradigm (**g**). **c**,**h**, Social interaction time in the absence or presence of social target. Two-way ANOVA in **c**, $F_{(1,40)}$=5.316, P=0.0259, n=12, 12 mice, respectively. Two-way ANOVA in **h**, $F_{(1,36)}$=7.301, P=0.0104, n=8, 10 mice, respectively. **d** and **i**, Sucrose preference in SPT. Two-sided unpaired t-test in **d**, t=2.677, d.f.=22, P=0.0259, n=12, 12 mice, respectively. Two-sided unpaired t-test in **i**, t=4.002, d.f.=20, P=0.0259, n=8, 14 mice, respectively. **e**,**j**, Total immobility time in TST. Two-sided unpaired t-test in **e**, t=3.229, d.f.=22, P=0.0259, n=12, 12 mice. Two-sided unpaired t-test in **j**, t=4.597, d.f.=20, P=0.0259, n=8, 14 mice. **k–m**, Representative traces (**k**) of cell-attached slice recording from BLA CCK neurons expressing hM3Dq-mCherry that was silenced by application of CNO (5 μM, 50 s). CNO induced rapid depolarization of membrane potential (**l**) and greatly increased firing rate (**m**), but did not affect membrane potential and firing rates of neurons expressing only mCherry (control). Two-way ANOVA in **l** (left), $F_{(1,8)}$=53.37, P<0.0001. Two-sided unpaired t-test in **l** (right), t=7.306, d.f.=8, P<0.0001. Two-way ANOVA in **m**, $F_{(1,8)}$=295.2, P<0.0001. n=5, 5 neurons, each from 3 mice for mCherry and hM3Dq groups, respectively. All data are mean ± s.e.m. **P<0.01; ***P<0.001; ****P<0.0001; n.s., no significance.

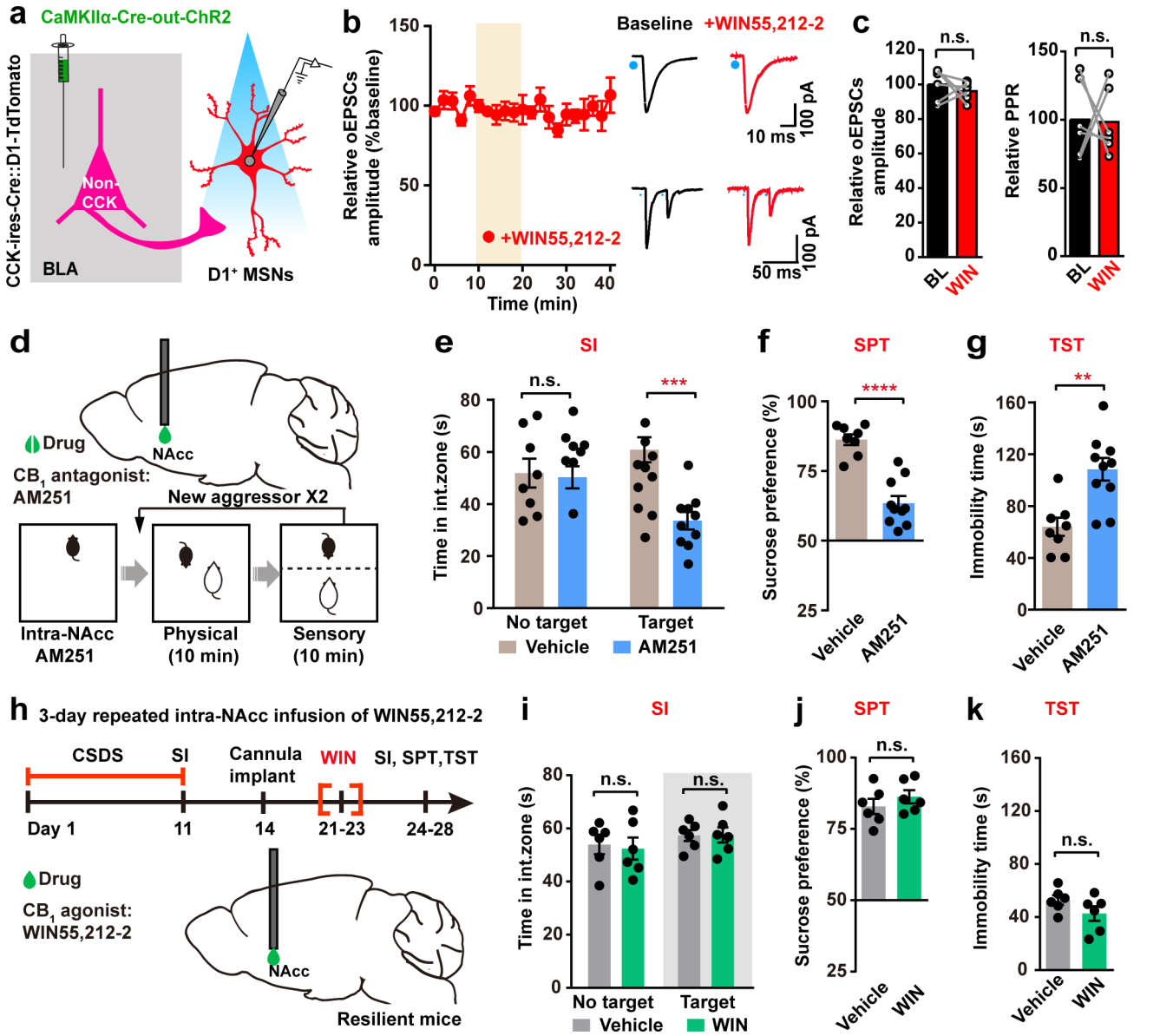

Extended Data Fig. 8 | Absence of CB_1R in non-CCK^{BLA}–$D1^{NAcc}$ circuit and modulation of CB_1R on stress susceptibility. a, Schematic of virus injection to express CaMKIIα-Cre-out-ChR2-eYFP in BLA of CCK-ires-Cre::D1-tdTomato mice and in vitro slice recording in D1-tdTomato-positive ($D1^+$) neurons in NAcc. **b**, Left, normalized oEPSCs following application of CB_1 agonist WIN55,212-2 (10 min, 1 μM). Right, representative traces of oEPSCs (top) and 50 ms PPR (bottom) in absence (left) and presence (right) of WIN55,212-2. **c**, Left, relative (% normalized to baseline) BLA non-CCK to D1 oEPSC amplitude (top) and 50 ms PPR (right) following WIN55,212-2 application (10 min, 1 μM). Two-sided paired *t*-test in **c** (left), $t = 0.7557$, d.f. = 5, $P = 0.4839$. Two-sided paired *t*-test in **c** (right), $t = 0.8358$, d.f. = 5, $P = 0.9366$. $n = 6$ neurons from 3 mice. **d**, Schematic of local bilateral infusion of AM251 (0.5 μg, 100 μl each side) into NAcc during two-trial SSDS. **e–g**, Effect of local bilateral infusion of AM251 into NAcc during SSDS on social interaction time (**e**), SPT (**f**) and TST (**g**), Two-way ANOVA in **e**, $F_{(1,32)} = 8.067$, $P = 0.078$; two-sided unpaired *t*-test in **f**, $t = 6.686$, d.f. = 16, $P < 0.0001$; two-sided unpaired *t*-test in **g**, $t = 3.810$, d.f. = 16, $P = 0.0015$. $n = 8$, 10 mice, respectively. **h,** Paradigms of 3-day repeated intra-NAcc local infusion of WIN55,212-2 (0.5 μg, 100 μl each side) in susceptible mice following 10 days of CSDS. **i**, Social interaction time in absence or presence of social target. Two-way ANOVA, $F_{(1,20)} = 0.06534$, $P = 0.8009$, $n = 6$, 6 mice for each group, respectively. **j**, Sucrose preference in SPT. Two-sided unpaired *t*-test, $t = 0.9594$, d.f. = 10, $P = 0.3600$, $n = 6$, 6 mice for each group, respectively. **k**, Total immobile time in TST. Two-sided unpaired *t*-test, $t = 1.548$, d.f. = 10, $P = 0.1527$, $n = 6$, 6 mice for each group, respectively. All data are means ± s.e.m. $^{**}P < 0.01$; $^{***}P < 0.001$; $^{****}P < 0.0001$; n.s., no significance.

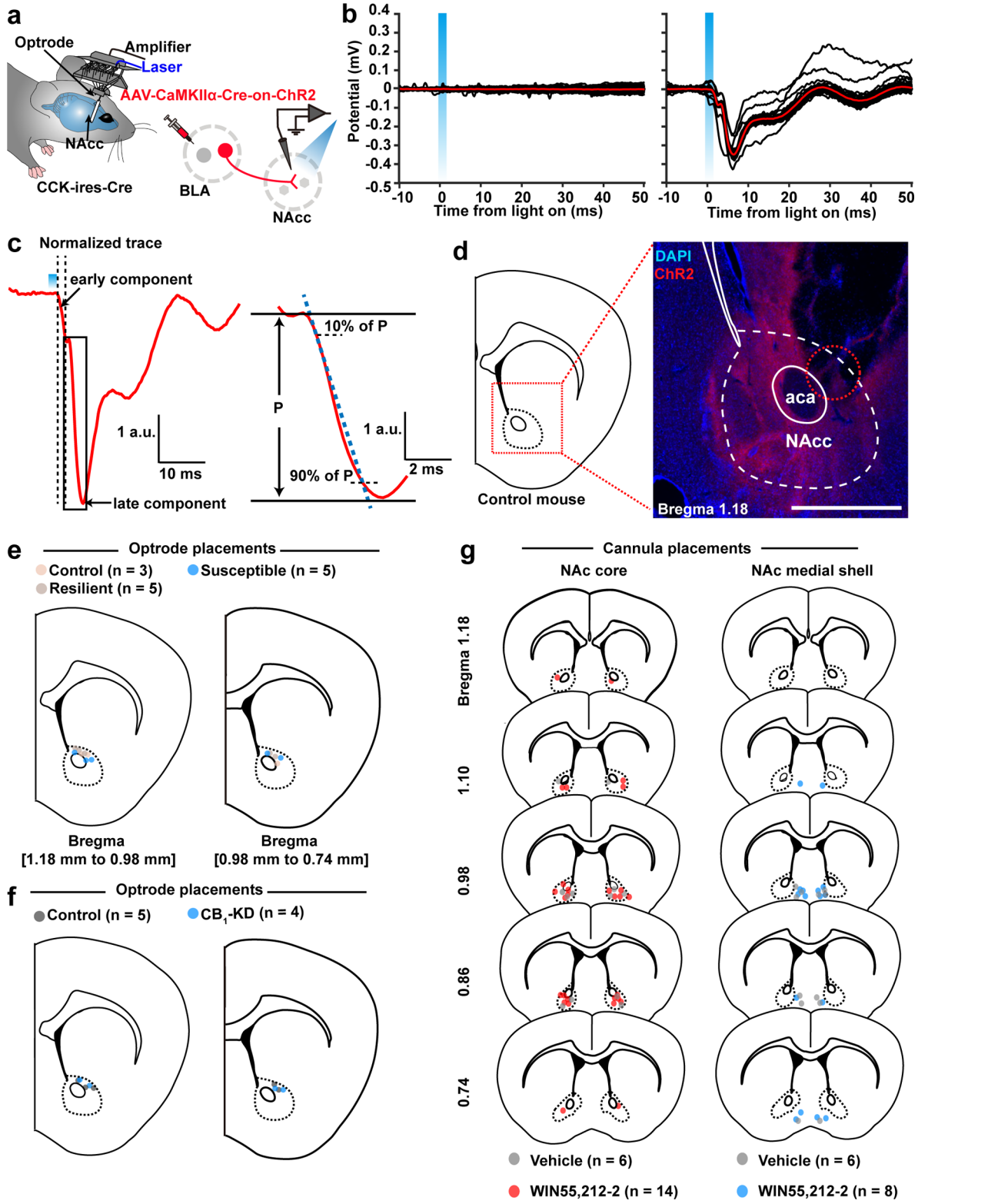

Extended Data Fig. 9 | In vivo fEPSP recordings of synaptic strength in CCK$^{BLA\text{-}NAcc}$ circuit and histological verification of optrode/cannula placement. a, Recording method used to examine CCK$^{BLA\text{-}NAcc}$ synaptic strength in vivo. **b**, fEPSPs aligned to light stimulation from recordings in NAcc of anaesthetized mice without (left) and with (right) ChR2 expressed in BLA. Each light-evoked fEPSP is shown as a black trace, with the red trace representing the average. **c**, Left, normalized fEPSP trace evoked by photostimulation, comprising an early component (reflecting light-evoked ChR2 currents in BLA CCK axon terminals) and a late component (reflecting postsynaptic responses in NAcc). Data were normalized to the peak of the first component. Right, rising phase of late component of fEPSPs (10–90% of peak, P) was fitted linearly with the slope of the fit, a good measure of synaptic strength, used for quantification of light-evoked fEPSPs. **d**, Example placement of optrode in NAcc; circle indicates tip of the optrode. Dashed white lines are boundaries of subregions; scale bar, 1 mm. **e–g**, Placement of all optrodes and cannulae.

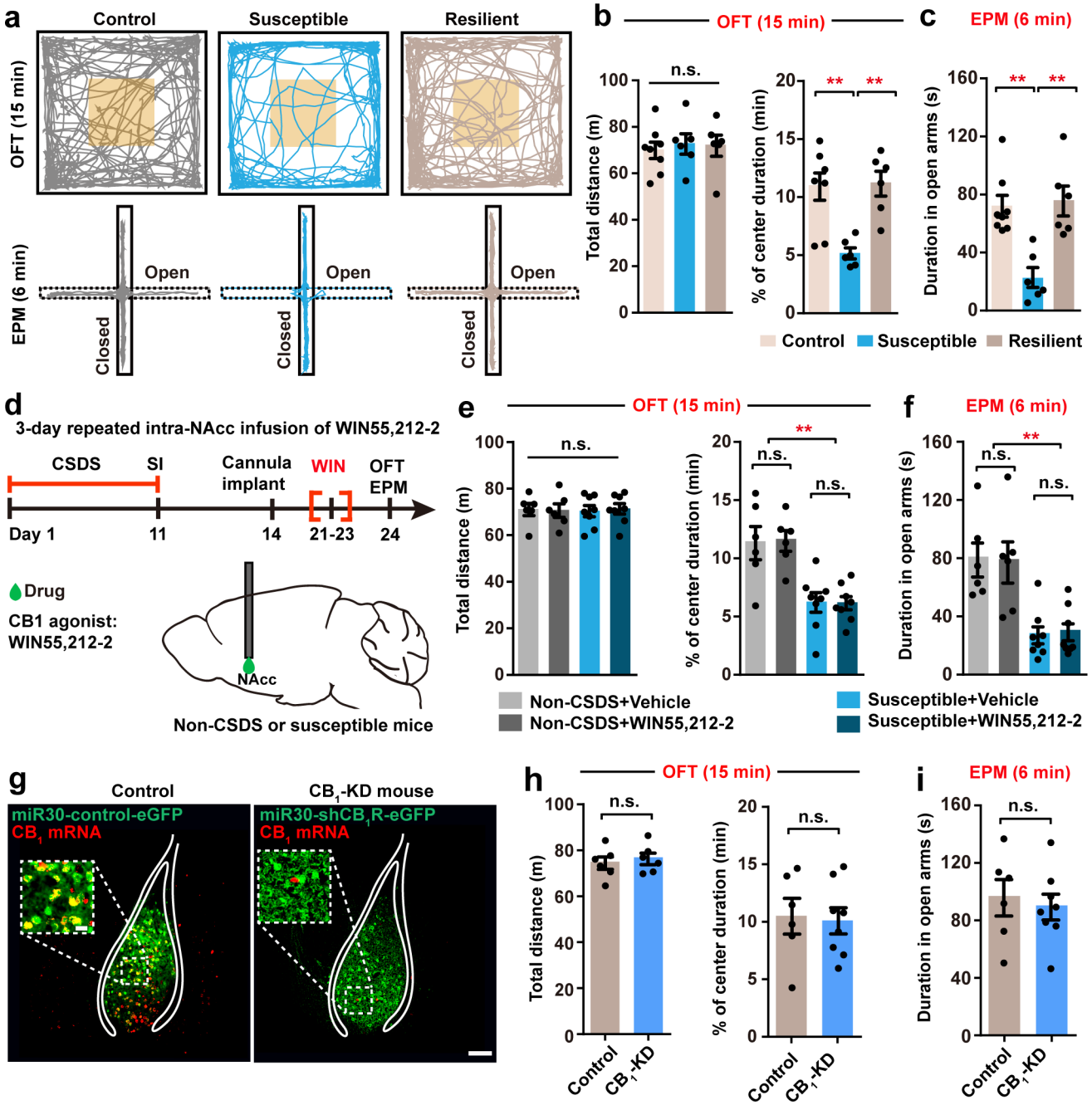

Extended Data Fig. 10 | CB_1R manipulation in CCK^{BLA}–$D2^{NAcc}$ circuit does not alter anxiety-like behavior. a, Representative animal tracks in open-field test (OFT, top) and elevated plus maze (EPM, bottom). **b**,**c**, Quantification of total distance, percentage of center duration in OFT (**b**) and open arms duration in EPM (**c**), showing that susceptible mice exhibited anxiety-like behavior. One-way ANOVA in **b** (total distance), $F_{(2, 17)}=0.1236$, $P=0.8845$. One-way ANOVA in **b** (% center duration), $F_{(2, 17)}=10.39$, $P=0.0011$. One-way ANOVA in **c**, $F_{(2, 17)}=11.79$, $P=0.0006$. $n=8, 6, 6$ mice for each group, respectively. **d**, Paradigm of 3-day repeated intra-NAcc local infusion of WIN55,212-2 (0.5 μg, 100 μl each side) in susceptible mice following 10-day CSDS. **e**,**f**, 3-day repeated intra-NAcc local infusion of WIN55,212-2 (0.5 μg, 100 μl each side) did not rescue anxiety-like behavior in susceptible mice. One-way ANOVA in **e** (total distance), $F_{(3, 24)}=0.03388$, $P=0.9914$. One-way ANOVA in **e** (% center duration), $F_{(3, 24)}=10.52$, $P=0.0001$. One-way ANOVA in **f**, $F_{(3, 24)}=9.728$, $P=0.0002$. $n=6, 6, 8, 8$ mice for each group, respectively. **g**, Representative images of BLA miR30-control-eYFP and miR30-shCB$_1$R-eGFP virus expression in control and CB_1-KD mice, co-labeled with CB_1 mRNA; scale bar, 200 μm. Inset, magnified view of the rectangular region in BLA; scale bar, 20 μm. **h**,**i**, Anxiety-like behavior in mice with expression of various viral constructs in BLA. Two-sided unpaired *t*-test in **h** (total distance), $t=0.5039$, d.f. $=10$, $P=0.6252$; Two-sided unpaired *t*-test in **h** (% center duration), $t=0.2156$, d.f. $=10$, $P=0.8329$; Two-sided unpaired *t*-test in **i**, $t=0.4314$, d.f. $=10$, $P=0.6738$. $n=6, 6$ mice, respectively. All data are means ± s.e.m. $^{**}P<0.01$; n.s., no significance.

nature research

Corresponding author(s): Xiao-Ming Li

Reporting Summary

Nature Research wishes to improve the reproducibility of the work that we publish. This form provides structure for consistency and transparency in reporting. For further information on Nature Research policies, see Authors & Referees and the Editorial Policy Checklist.

Statistical parameters

When statistical analyses are reported, confirm that the following items are present in the relevant location (e.g. figure legend, table legend, main text, or Methods section).

n/a	Confirmed	
☐	☒	The exact sample size (*n*) for each experimental group/condition, given as a discrete number and unit of measurement
☐	☒	An indication of whether measurements were taken from distinct samples or whether the same sample was measured repeatedly
☐	☒	The statistical test(s) used AND whether they are one- or two-sided *Only common tests should be described solely by name; describe more complex techniques in the Methods section.*
☐	☒	A description of all covariates tested
☐	☒	A description of any assumptions or corrections, such as tests of normality and adjustment for multiple comparisons
☐	☒	A full description of the statistics including central tendency (e.g. means) or other basic estimates (e.g. regression coefficient) AND variation (e.g. standard deviation) or associated estimates of uncertainty (e.g. confidence intervals)
☐	☒	For null hypothesis testing, the test statistic (e.g. *F*, *t*, *r*) with confidence intervals, effect sizes, degrees of freedom and *P* value noted *Give P values as exact values whenever suitable.*
☒	☐	For Bayesian analysis, information on the choice of priors and Markov chain Monte Carlo settings
☒	☐	For hierarchical and complex designs, identification of the appropriate level for tests and full reporting of outcomes
☐	☒	Estimates of effect sizes (e.g. Cohen's *d*, Pearson's *r*), indicating how they were calculated
☐	☒	Clearly defined error bars *State explicitly what error bars represent (e.g. SD, SE, CI)*

Our web collection on statistics for biologists may be useful.

Software and code

Policy information about availability of computer code

Data collection	The patch-clamp data were collected using pCLAMP 10 (Axon Instruments). Mice behaviour were recorded using Anymaze software (Stoelting). The in-vivo electrophysiological signals were acquired using OmniPlex (Plexon).
Data analysis	GraphPad Prism 6.01, SPSS statistics V19.0, MATLAB R2014a, Spike2 6.11, Anilab software, MiniAnalysis, Image J Fiji. Custom Matlab code will be available upon request, Microsoft Excel 2016

For manuscripts utilizing custom algorithms or software that are central to the research but not yet described in published literature, software must be made available to editors/reviewers upon request. We strongly encourage code deposition in a community repository (e.g. GitHub). See the Nature Research guidelines for submitting code & software for further information.

Data

Policy information about availability of data

All manuscripts must include a data availability statement. This statement should provide the following information, where applicable:

- Accession codes, unique identifiers, or web links for publicly available datasets
- A list of figures that have associated raw data
- A description of any restrictions on data availability

The datasets generated during and/or analysed during the current study are available from the corresponding author on reasonable request.

Field-specific reporting

Please select the best fit for your research. If you are not sure, read the appropriate sections before making your selection.

☒ Life sciences ☐ Behavioural & social sciences ☐ Ecological, evolutionary & environmental sciences

For a reference copy of the document with all sections, see nature.com/authors/policies/ReportingSummary-flat.pdf

Life sciences study design

All studies must disclose on these points even when the disclosure is negative.

Sample size	We did not use statistical methods to predetermine sample sizes, but our sample sizes are similar to those generally employed in the field.
Data exclusions	For all experiments, the animals' brain were processed for histology to confirm virus infection sites. Data will be excluded if the infection sites were off from the desired nuclei. The exclusion criteria were pre-determined before any experiment.
Replication	All studies have been repeated at least twice with similar results. To ensure experimental findings can be easily reproduced, we included detailed methods in the manuscript.
Randomization	Mice were randomly assigned to treatments, all mice were assigned to stress-susceptible (SS) or resilient (RES) groups based on their behavioral profile when compared to unstressed controls. Samples were taken from all animals used in this study.
Blinding	All behavioral scoring, c-fos numbers counting and western blot analysing were down blind to the treatment groups.

Reporting for specific materials, systems and methods

Materials & experimental systems

n/a	Involved in the study
☒	☐ Unique biological materials
☐	☒ Antibodies
☒	☐ Eukaryotic cell lines
☒	☐ Palaeontology
☐	☒ Animals and other organisms
☒	☐ Human research participants

Methods

n/a	Involved in the study
☒	☐ ChIP-seq
☒	☐ Flow cytometry
☒	☐ MRI-based neuroimaging

Antibodies

Antibodies used

Primary antibodies:
Anti-GAD67, mouse, Millipore, cat. no. MAB5406, 1:400 diluted
Anti-PV, rabbit, Swant , cat. no. pv27, 1:5000 diluted
Anti-SOM, rabbit, Millipore, cat. no. MAB354, 1:200 diluted
Anti-CaMKIIα, rabbit, Abcam, cat. no. ab52476, 1:1000 diluted
Anti-c-fos, rabbit, Millipore, cat. no. PC38, 1:5000 diluted
Anti-Cav2.1, rabbit, Abcam, cat. no. ab181371, 1:1000 diluted
Anti-SNAP25, rabbit, Abcam, cat. no. ab5666, 1:1000 diluted
Anti-RIM3, rabbit, Abcam, cat. no. ab192602, 1:1000 diluted
Anti-CB1R, rabbit, Epitomics, cat. no. 8063-1, 1:1000 diluted
Anti-GAPDH, rabbit, Cell Signaling Technology, cat. no. 5174, 1:5000 diluted

Secondary antibodies:
Alexa Fluor 488-conjugated anti-rabbit (1:400, Invitrogen, R37118)
Alexa Fluor 555-conjugated anti-rabbit (1:400, Invitrogen, A32794)
Alexa Fluor 488-conjugated anti-mouse (1:400, Invitrogen, R37114)
Alexa Fluor 555-conjugated anti-mouse (1:400, Invitrogen, A32727)
Alexa Fluor 633-conjugated streptavidin (1:1000, Invitrogen, S21375)
DAPI (1:1000, Invitrogen, D1306)
Goat Anti-Rabbit IgG H&L (HRP) (1:3000, Abcam, ab136817)

RNAscope:
Cnr 1-C1 probe: GenBank accession number NM_007726.3; target nt region, 530 - 1458
Drd 2-C1 probe: GenBank accession number NM_010077.2; target nt region, 69 - 1175
CCK-C2 probe: GenBank accession number NM_031161.3; target nt region, 23 - 679
Rspo-C1 probe: GenBank accession number NM_172815.3; target nt region, 537 - 1452
Drd1-C2 probe: GenBank accession number NM_010076.3; target nt region, 521 - 1524
Ppp1r1b-C3 probe: GenBank accession number NM_144828.1; target nt region, 590 - 1674

Validation

All antibodies are validated for species by manufacturer

Animals and other organisms

Policy information about studies involving animals; ARRIVE guidelines recommended for reporting animal research

Laboratory animals

Male C57BL/6J mice (about 25 g) were purchased at 7 weeks of age from Shanghai SLAC Laboratoy and allowed one week of acclimation to the Zhejiang University house facilities before the start of experiments. Retired male CD-1 breeders (about 40 g) of at least 4 months age were purchased from Beijing Charles River Laboratories and used as aggressors.

Wild animals

This study did not involve wild animals.

Field-collected samples

This study did not involve samples collected from the field.